



University of Dundee

### Discovery and Optimization of 5-Amino-1,2,3-triazole-4-carboxamide Series against *Trypanosoma cruzi*

Brand, Stephen; Ko, Eun Jung; Viayna, Elisabet; Thompson, Stephen; Spinks, Daniel; Thomas, Michael; Sandberg, Lars; Francisco, Amanda F.; Jayawardhana, Shiromani; Smith, Victoria C.; Jansen, Chimed; De Rycker, Manu; Thomas, John; MacLean, Lorna; Osuna-Cabello, Maria; Riley, Jennifer; Scullion, Paul; Stojanovski, Laste; Simeons, Frederick; Epemolu, Rafiu; Shishikura, Yoko; Crouch, Sabrina D.; Bakshi, Tania S.; Nixon, Christopher J.; Reid, Iain H.; Hill, Alan P.; Underwood, Tim Z.; Hindley, Sean J.; Robinson, Sharon A.; Kelly, John M.; Fiandor, Jose M.; Wyatt, Paul G.; Marco, Maria; Miles, Timothy J.; Read, Kevin D.; Gilbert, Ian

*Published in:*  
Journal of Medicinal Chemistry

*DOI:*  
[10.1021/acs.jmedchem.7b00463](https://doi.org/10.1021/acs.jmedchem.7b00463)

*Publication date:*  
2017

*Document Version*  
Publisher's PDF, also known as Version of record

[Link to publication in Discovery Research Portal](#)

*Citation for published version (APA):*

Brand, S., Ko, E. J., Viayna, E., Thompson, S., Spinks, D., Thomas, M., ... Gilbert, I. H. (2017). Discovery and Optimization of 5-Amino-1,2,3-triazole-4-carboxamide Series against *Trypanosoma cruzi*. *Journal of Medicinal Chemistry*, 60(17), 7284-7299. DOI: 10.1021/acs.jmedchem.7b00463

## Discovery and Optimization of 5-Amino-1,2,3-triazole-4-carboxamide Series against *Trypanosoma cruzi*

Stephen Brand,<sup>†</sup> Eun Jung Ko,<sup>†</sup> Elisabet Viayna,<sup>†</sup> Stephen Thompson,<sup>†</sup> Daniel Spinks,<sup>†</sup> Michael Thomas,<sup>†</sup> Lars Sandberg,<sup>†</sup> Amanda F. Francisco,<sup>‡</sup> Shiromani Jayawardhana,<sup>‡</sup> Victoria C. Smith,<sup>†</sup> Chimed Jansen,<sup>†</sup> Manu De Rycker,<sup>†,§</sup> John Thomas,<sup>†</sup> Lorna MacLean,<sup>†</sup> Maria Osuna-Cabello,<sup>†</sup> Jennifer Riley,<sup>†</sup> Paul Scullion,<sup>†</sup> Laste Stojanovski,<sup>†</sup> Frederick R. C. Simeons,<sup>†</sup> Ola Epemolu,<sup>†</sup> Yoko Shishikura,<sup>†</sup> Sabrina D. Crouch,<sup>§</sup> Tania S. Bakshi,<sup>||</sup> Christopher J. Nixon,<sup>||</sup> Iain H. Reid,<sup>⊥</sup> Alan P. Hill,<sup>⊥</sup> Tim Z. Underwood,<sup>⊥</sup> Sean J. Hindley,<sup>⊥</sup> Sharon A. Robinson,<sup>#</sup> John M. Kelly,<sup>‡</sup> Jose M. Fiandor,<sup>§</sup> Paul G. Wyatt,<sup>†</sup> Maria Marco,<sup>§</sup> Timothy J. Miles,<sup>\*,§</sup> Kevin D. Read,<sup>\*,†</sup> and Ian H. Gilbert<sup>\*,†,§</sup>

<sup>†</sup>Drug Discovery Unit, Division of Biological Chemistry and Drug Discovery, College of Life Sciences, University of Dundee, Sir James Black Centre, Dundee DD1 5EH, U.K.

<sup>‡</sup>Department of Pathogen Molecular Biology, London School of Hygiene and Tropical Medicine, Keppel Street, London WC1E 7HT, U.K.

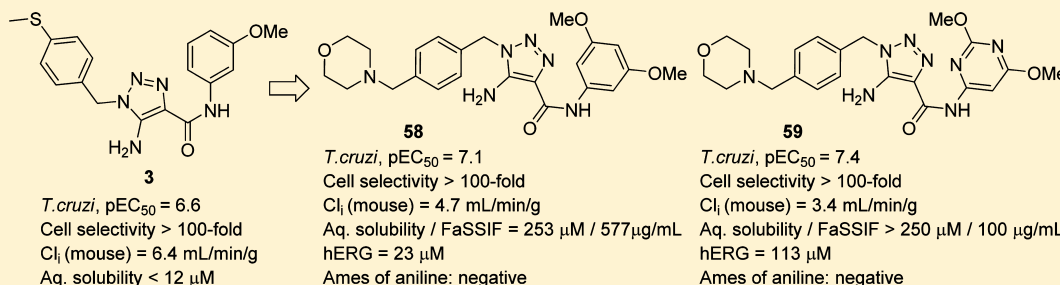
<sup>§</sup>Diseases of the Developing World, GlaxoSmithKline, Calle Severo Ochoa 2, 28760 Tres Cantos, Madrid, Spain

<sup>||</sup>GlaxoSmithKline, 1250 South Collegeville Road, PO Box 5089, Collegeville, Pennsylvania 19426-0989, United States

<sup>⊥</sup>Medicines Research Centre, GlaxoSmithKline, Gunnels Wood Road, Stevenage, Hertfordshire SG1 2NY, U.K.

<sup>#</sup>David Jack Centre for R&D, GlaxoSmithKline, Park Road, Ware, Hertfordshire SG12 0DP, United Kingdom

### Supporting Information



**ABSTRACT:** Chagas' disease, caused by the protozoan parasite *Trypanosoma cruzi*, is the most common cause of cardiac-related deaths in endemic regions of Latin America. There is an urgent need for new safer treatments because current standard therapeutic options, benznidazole and nifurtimox, have significant side effects and are only effective in the acute phase of the infection with limited efficacy in the chronic phase. Phenotypic high content screening against the intracellular parasite in infected VERO cells was used to identify a novel hit series of 5-amino-1,2,3-triazole-4-carboxamides (ATC). Optimization of the ATC series gave improvements in potency, aqueous solubility, and metabolic stability, which combined to give significant improvements in oral exposure. Mitigation of a potential Ames and hERG liability ultimately led to two promising compounds, one of which demonstrated significant suppression of parasite burden in a mouse model of Chagas' disease.

### INTRODUCTION

Chagas' disease,<sup>1</sup> caused by the protozoan parasite *Trypanosoma cruzi* is a leading cause of cardiac related deaths in endemic regions of Central and South America.<sup>2,3</sup> It is estimated that 5–8 million people are currently infected with the parasite, many of them unknowingly, and that the disease causes over 10,000 deaths per year.<sup>4</sup> The parasite is primarily transmitted via the faeces of the blood-sucking “kissing” bug<sup>5</sup> (triatomine bug of the Reduviid order), which proliferates in poor housing conditions. The parasite enters the body through the bite site wound or through mucosal membranes, although cases of transmission through blood transfusions,<sup>6</sup> eating contaminated

food or drink,<sup>7</sup> organ donation,<sup>8</sup> breast feeding,<sup>9</sup> and the congenital route are widely documented. Increasingly, due to migration of Latin American immigrants who unknowingly carry the parasite in their blood, patient numbers are growing in nonendemic countries including Australia, Canada, Japan, Spain, and the United States.<sup>10</sup>

The disease has two distinct phases, both of which can be hard to detect. There is a short acute phase, during which blood parasite levels are relatively high, which although typically

Received: March 30, 2017

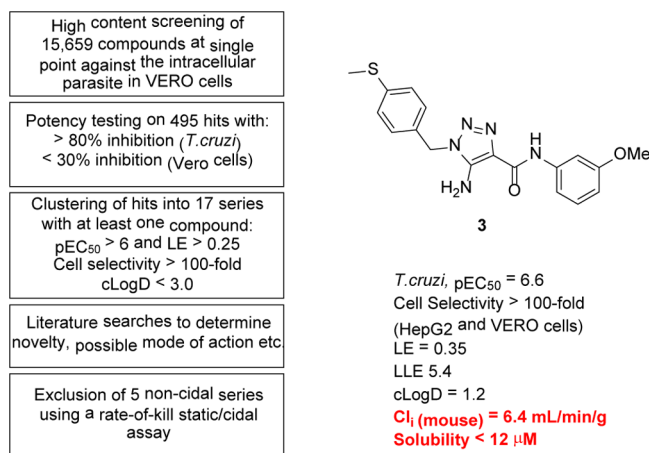
Published: August 27, 2017

associated with mild symptoms such as fever, body aches, malaise, and vomiting, causes death in approximately 5% of diagnosed children. This is followed by the chronic indeterminate or "silent" stage<sup>11</sup> which may span decades,<sup>12</sup> during which infected people may spontaneously clear the infection or reduce it to undetectable levels and not present clinical symptoms. However, if left untreated, up to 30% of chronically infected people will go on to suffer irreversible damage to the heart, esophagus, and/or colon,<sup>13</sup> ultimately leading to severe disability or death.<sup>14</sup>

The nitro compounds benznidazole (BNZ, **1**) and nifurtimox (**2**), which are not FDA approved, are the most commonly used drugs to treat *T. cruzi* infection.<sup>15</sup> However, they cause significant side effects<sup>16</sup> and are only proven to be effective in the acute phase of the infection with limited efficacy in the chronic phase of the infection.<sup>17–19</sup> Furthermore, in patients with Chagas' cardiomyopathy although trypanocidal therapy with benznidazole (**1**) does significantly reduce serum parasite detection, after five years there is no significant effect on cardiac clinical deterioration.<sup>20</sup> There is therefore an urgent need for affordable drugs which have a superior safety and efficacy profile, which do not require hospitalization, and are suitable for tropical climates.

## HIT DISCOVERY

To identify new chemical start points, a phenotypic screen was performed on a small diversity collection,<sup>21</sup> a nonbiased diversity library containing 15659 lead-like compounds, using a high-content assay which measures inhibition of proliferation of intracellular transgenic *Trypanosoma cruzi* parasites (Silvio X10/7 clone A1 strain) in VERO cells.<sup>22</sup> Compounds were initially tested at a single concentration (15  $\mu$ M) over 3 days. The potency of suitable hits ( $n = 495$ ), defined as those which exhibited >80% inhibition of parasite growth and <30% inhibition of growth of VERO cells, was then determined by 10-point dose response (potency range 0.0025–50  $\mu$ M). Compounds were manually clustered into series according to their core scaffolds, and those series containing exemplars with desirable properties, i.e., potency ( $pEC_{50} > 6$ ), cellular ligand efficiency<sup>23,24</sup> ( $LE > 0.25$ ), cell selectivity (>100-fold over VERO and HepG2 cells), and calculated lipophilicity ( $cLogD < 3$ ), were progressed. All series which were not cidal, or which had been the subject of previously reported studies, were subsequently excluded.<sup>25–31</sup> The screening cascade is shown in Figure 1.<sup>22</sup>



**Figure 1.** Screening cascade and biological and physicochemical profile of screening hit **3**.

Twelve hit series were originally identified which met our own progression criteria as well as being in-line with Drugs for Neglected Diseases *initiative* (DNDi) requirements.<sup>32,33</sup> Compound **3** was the most potent representative of a series of compounds containing the 5-amino-1,2,3-triazole-4-carboxamide (ATC) core and had submicromolar activity ( $pEC_{50} > 6$ ), which was confirmed upon retesting resynthesized material. Literature searching indicated the ATC core was highly novel, with very little precedent in medicinal chemistry programmes.

This series was prioritized for optimization based on a comparison of the activity, selectivity, and ligand efficiency profiles of all 12 trypanocidal hit series identified from this screen. Although compound **3** only had moderate potency against the parasite, it had high ligand efficiency ( $LE = 0.35$ ), good lipophilic ligand efficiency<sup>34,35</sup> ( $LLE = (pEC_{50} - cLogD) = 5.4$ ), and cell selectivity (>100-fold against VERO and HepG2 cells). The compound had poor metabolic stability when incubated with mouse liver microsomes and poor kinetic aqueous solubility. The aim was therefore to identify a more potent drug-like compound with an acceptable physicochemical and DMPK profile suitable for evaluation in acute and chronic animal models of Chagas' disease.

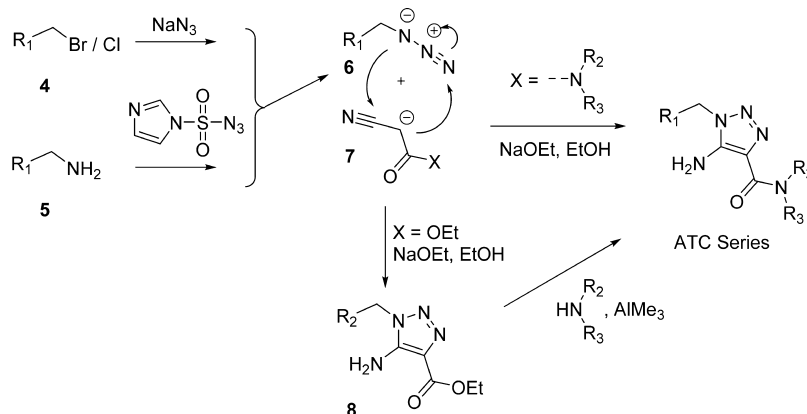
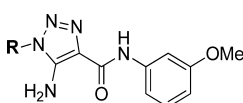
## STRUCTURE–ACTIVITY RELATIONSHIPS AND HIT TO LEAD STUDIES

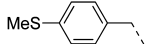
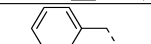

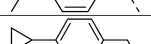
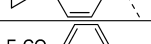
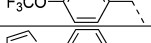
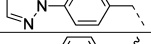
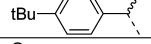

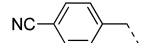
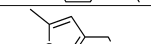
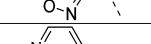
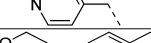
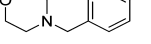
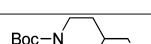
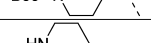
We first explored which of the pharmacophoric elements of the ATC scaffold were associated with activity by performing some simple modifications and deletions, and these indicated the core was not susceptible to optimization through a scaffold hopping approach. For example, a compound where the amino group related to **3** was replaced with H, Me, Cl, or NMe<sub>2</sub> were inactive (see Supporting Information, Table S1). This could suggest that the intramolecular hydrogen bond between the NH<sub>2</sub> and amide carbonyl oxygen might be required for maintaining the bioactive conformation or that the NH<sub>2</sub> group makes a specific interaction with the molecular target. Modifications of the central triazole to either an imidazole or pyrazole also led to loss of activity (see Supporting Information, Table S2).

Optimization of this series therefore focused on adjustment of peripheral substituents around this core. Rapid exploration of structure–activity relationships (SAR) was made possible because analogues could be synthesized expediently either via cyclization of an azide with an  $\alpha$ -cyano amide<sup>36</sup> (**7**, X = NR<sub>2</sub>R<sub>3</sub>) or by Lewis-acid catalyzed (AlMe<sub>3</sub>) amination<sup>37</sup> of the ethyl ester (**8**), prepared by cyclization of an azide (**6**) with ethyl-2-cyanoacetate (see Scheme 1). The azide intermediates were conveniently accessed either by reaction of alkyl or benzyl halides with sodium azide or from the corresponding primary amine by diazo transfer with 1*H*-imidazole-1-sulfonyl azide hydrochloride.<sup>38</sup>

Compound **3** would likely have poor oral exposure due to its poor metabolic stability (high intrinsic clearance when incubated with mouse liver microsomes,  $Cl_i = 6.4 \text{ mL min}^{-1} \text{ g}^{-1}$ ) and was therefore not progressed to in vivo pharmacokinetics. Metabolite ID following incubation with mouse liver microsomes (at 0.5 and 5.0  $\mu$ M for 30 min) indicated rapid formation of a principal metabolite arising from oxidation on the benzyl subunit, assumed to be the corresponding sulfoxide **16** which is significantly less active, followed by further oxidation on the benzamide ring. Work therefore focused on modifications at the *para*-position of the benzyl ring to improve the metabolic stability and probe for additional potency (see Table 1). This revealed that activity was very significantly dependent upon the nature of the substituent.

Scheme 1. Generalized Synthetic Routes to 5-Amino-1,2,3-triazole-4-carboxamides

Table 1. Modifications to the *N*-Benzyl Substituent


R	Compound	<i>T. cruzi</i> pEC <sub>50</sub> <sup>a</sup>	VERO pEC <sub>50</sub> <sup>a</sup>	Cl <sub>i</sub> <sup>b</sup> (mouse)	Solubility <sup>c</sup> (μM)	Chi LogD, (PFI)
Reference compounds	Benzidazole ( <b>1</b> )	5.5	< 4.3	nd	nd	nd
	Nifurtimox ( <b>2</b> )	5.9	< 4.3	nd	nd	nd
	Posaconazole ( <b>9</b> )	8.7	< 6.0	nd	56	nd
MeS- 	<b>3</b>	6.6	< 4.3	6.4	< 12	nd
	<b>10</b>	5.2	< 4.3	3.7	16	2.6 (7.6)
	<b>11</b>	7.4	< 4.3	3.2	14	3.4 (8.9)
	<b>12</b>	7.0	< 4.3	4.9	79	3.2 (8.6)
F <sub>3</sub> CO- 	<b>13</b>	7.4	< 4.3	2.9	12	3.6 (9.3)
	<b>14</b>	6.7	< 4.3	2.3	20	2.4 (7.3)
tBu- 	<b>15</b>	8.1	4.4	nd	20	3.9 (9.8)
	<b>16</b>	4.4	< 4.3	0.5	> 250	1.3 (5.5)
NC- 	<b>17</b>	5.3	< 4.3	2.5	216	2.3 (7.2)
	<b>18</b>	< 4.3	< 4.3	2.6	174	2.0 (6.7)
	<b>19</b>	4.8	< 4.3	0.7	< 12	1.4 (5.7)
	<b>20</b>	7.0	< 4.3	3.6	> 250	2.2 (7.0)
Boc-N- 	<b>21</b>	5.7	< 4.3	10	39	2.9 (7.1)
HN- 	<b>22</b>	< 4.3	< 4.3	< 0.5	> 250	0.6 (3.4)
Ac-N- 	<b>23</b>	< 4.3	< 4.3	0.7	> 250	1.2 (4.4)
	<b>24</b>	6.1	4.9	nd	nd	nd

<sup>a</sup>pEC<sub>50</sub> values are shown as mean values from two or more EC<sub>50</sub> determinations. Standard deviation is typically within 2-fold from the EC<sub>50</sub>.  
<sup>b</sup>Cl<sub>i</sub> when incubated with liver microsomes; mL min<sup>-1</sup> g<sup>-1</sup>. <sup>c</sup>Kinetic aqueous solubility at pH 7.4 measured by nephelometry.

For instance, removal of the thiomethyl reduced activity more than 10-fold (i.e., **10**) while replacing the SMe with the larger isopropyl group improved activity by 10-fold (i.e., **11**, pEC<sub>50</sub> = 7.4), suggesting *para* substituents might be occupying a

hydrophobic binding pocket. Indeed, cyclopropyl (**12**), -OCF<sub>3</sub> (**13**), and pyrazole (**14**) groups all offered good activity which reiterated this trend, with the most potent compound from this series being the *para-tert-butyl-α-methylbenzyl*-substituted

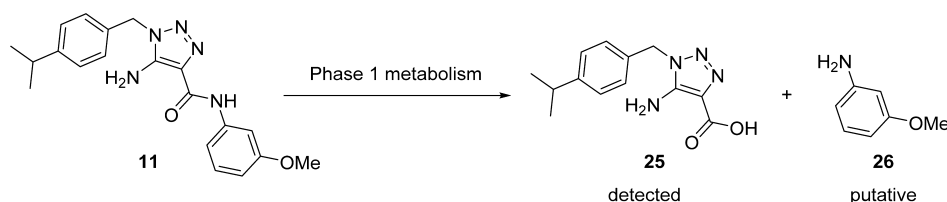


Figure 2. Metabolism of compound 11.

compound (**15**). In general, substituents investigated at the *para*-position of the benzyl ring improved metabolic stability compared to the thiomethyl substituent.

It was important to ensure that activity was not being driven predominantly by nonspecific hydrophobic interactions because this can frequently lead to compounds with poor physicochemical properties. The aim was to maintain LLE > 5 and cLogD < 3. In fact, calculated values of LogD and LLE (Stardrop version 6.0, [www.optibrium.com](http://www.optibrium.com)) appeared to be well within acceptable limits even for the most active compounds; all compounds in Table 1 have cLogD < 2.2, and those with  $pEC_{50} > 6$  have LLE > 5. However, it was hypothesized that cLogD might be underestimating the true lipophilicity, due to the effects of intramolecular hydrogen bonding (in this case between the  $NH_2$  and the amide carbonyl oxygen) and the effects of the  $pK_a$  of the molecules.<sup>39</sup> Indeed comparison of LogD measured chromatographically with calculated LogD (i.e., ChiLogD<sup>40,41</sup> vs cLogD) of early compounds in this series suggested an underprediction (i.e., for **11** ChiLogD = 3.4, and cLogD = 1.7; for **13** ChiLogD = 3.6, and cLogD = 2.1; see Supporting Information, Figure S3 for a plot of ChiLogD vs cLogD). The higher than predicted lipophilicity was of concern as developability of compounds is negatively correlated with high lipophilicity. For example, the poor oral exposure of **11** and **13** (see below) is probably due to low solubility, which is likely to be driven in part by high lipophilicity.

Compounds **11** and **13** exhibited very poor exposure in mouse when dosed orally at 10 mg free base/kg ( $AUC_{0-8h} = 3200 \text{ ng}\cdot\text{min mL}^{-1}$  and  $2300 \text{ ng}\cdot\text{min mL}^{-1}$ ;  $C_{max} = 17$  and  $13 \text{ ng/mL}$ , respectively, see Supporting Information, Figures S5 and S6). In addition, **11**, when administered intraperitoneally (10 mg/kg), had very low blood exposure (<100 ng/mL) albeit with a long half-life, likely consistent with the slow release of a poorly soluble compound (aqueous solubility of **11** =  $14 \mu\text{M}$ , determined by both kinetic nephelometry and chemiluminescent nitrogen detection methods) from the peritoneal cavity. For both compounds, the poor oral exposure was likely driven by poor absorption due to the low solubility and moderate/high first pass metabolism ( $Cl_i$  in mouse liver microsomes  $3.2$  and  $2.9 \text{ mL min}^{-1}\text{g}^{-1}$ , respectively).

Further analysis showed there was evidence of hydrolysis of the amide in vivo of compound **11** to give the acid **25** (and presumably the corresponding aniline, **26**; Figure 2), which was detected in blood at approximately 25% of the level of parent (see Supporting Information, Figure S7).

In addition to high lipophilicity and low solubility, another potential concern over developability is the number of aromatic rings.<sup>42</sup> The property forecast index,<sup>43</sup>  $PFI = \text{ChromLogD}_{pH7.4} + \text{number of aromatic rings}$ , was therefore used as a parameter to guide optimization of aqueous solubility. (The  $\text{ChromLogD}_{pH7.4}$  is related to the chromatographically determined LogD through the equation  $\text{ChromLogD}_{pH7.4} =$

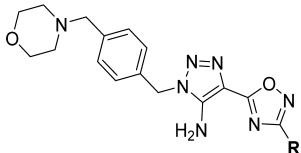
$[1.63\text{ChiLogD} + 0.396]$ , i.e.,  $PFI = [1.63\text{ChiLogD} + 0.396] + \text{number of aromatic rings}$ ).

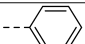
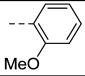
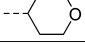
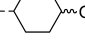
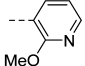
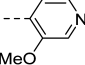
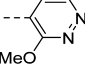
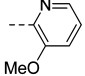
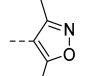
Because substituents at the benzyl *para*-position of **3** appeared to access a “sweet spot” at the target, efforts were focused first on modifying functionality in this position, seeking to strike a balance between the degree of lipophilicity required for good potency while minimizing LogD and/or number of aromatic rings (nAr), to help improve solubility. Even though solubility and metabolic stability were generally improved, a range of more polar modifications were found to significantly reduce activity, including: polar replacements of the *iPr* group of **11** (i.e., **16** and **17**), replacement of the benzyl ring with *para*-functionalized saturated ring systems (i.e., **21**, **22** and **23**), or methylhydroxylation of the benzylic position of **11** (i.e., **24**). Introduction of heteroatoms into the aromatic ring only led to a reduction in activity (i.e., **18** and **19**). Compound **20** (morpholine substituent), however, appeared to represent a promising lead because it had acceptable potency, selectivity, and moderate clearance, significantly reduced PFI relative to **11** (7.0 vs 8.9) and the pendant morpholine offered the additional advantage of using salt preparation to maximize solubility.<sup>44</sup> Investigation of alternative substitution patterns around the benzyl group showed that although a similar level of potency was maintained when the morpholine substituent was moved to the *meta*-position, a decrease in metabolic stability was observed compared to **20** (i.e., **S31** see Supporting Information, Table S4). Moving the morpholine substituent to the *ortho*-position led to a significant loss in potency (i.e., **S32** see Supporting Information, Table S4). Attempts to improve the profile of **20** with respect to potency, metabolic stability, and hERG inhibition, either by using alternative amines to the morpholine or applying different linkages between the morpholine and the triazole core, did not yield more suitable compounds and again demonstrated the apparent trend for substituents with higher polarity in this position to worsen potency (see Supporting Information, Table S3 and S4).

## LEAD OPTIMIZATION

Compound **20** exhibited a promising profile: cellular activity and selectivity were in line with our compound progression criteria and DMPK properties were reasonable; this included good thermodynamic solubility in physiologically relevant media, simulated intestinal fluid in the fasted state (FaSSIF =  $264 \mu\text{g/mL}$  for the HCl salt). The compound demonstrated moderate metabolic stability, with no significant off-target pharmacology (only one alert at  $pIC_{50} > 5$  in the GSK enhanced cross-screen panel (eXP) of enzymes, receptors, ion channels, and other liability targets)<sup>45,46</sup> and low inhibition of human CYP450s ( $IC_{50}$  for CYP1A2, 2C19, 2C9, 2D6, 3A4 isoforms  $>10 \mu\text{M}$ ). There were, however, two significant potential safety issues: (1) moderate inhibition of the hERG<sup>47</sup> potassium channel ( $IC_{50} = 24 \mu\text{M}$ , determined by Q-patch<sup>48</sup>), a potential cause of cardiac arrhythmia, and (2) the potential

Table 2. Optimization of the Oxadiazole Bioisostere



R	Compound	<i>T. cruzi</i> <sup>a</sup> pEC <sub>50</sub>	VERO pEC <sub>50</sub>	Cl <sub>i</sub> <sup>b</sup> (mouse)	Solubility <sup>c</sup> (μM)	Chi LogD (PFI)	hERG (μM)
	27	6.8	4.63	9.0	178 <sup>d</sup>	2.6 (8.6)	nd
	34	7.1	< 4.3	9.1	> 250 <sup>d</sup>	2.1 (7.8)	> 30
	35	< 4.3	< 4.3	0.8	> 250	1.3 (5.5)	nd
	36	< 4.3	< 4.3	2.1	> 250	0.9 (4.9)	nd
	37	7.1	< 4.3	3.3	> 250 <sup>d</sup>	1.7 (7.2)	> 30
	38	6.0	< 4.3	6.8	79	1.1 (6.2)	nd
	39	5.0	< 4.3	1.5	219	1.0 (6.0)	nd
	40	4.7	< 4.3	2.7	219 <sup>d</sup>	1.0 (5.8)	nd
	41	6.9	< 4.3	2.2	> 250 <sup>d</sup>	2.1 (7.8)	6

<sup>a</sup>pEC<sub>50</sub> values are shown as mean values from two or more EC<sub>50</sub> determinations. Standard deviation is typically within 2-fold from the EC<sub>50</sub>.  
<sup>b</sup>Cl<sub>i</sub> when incubated with liver microsomes; mL min<sup>-1</sup> g<sup>-1</sup>. <sup>c</sup>Kinetic aqueous solubility at pH 7.4 measured by nephelometry. <sup>d</sup>Kinetic aqueous solubility at pH 7.4 measured by nephelometry of the HCl salt.

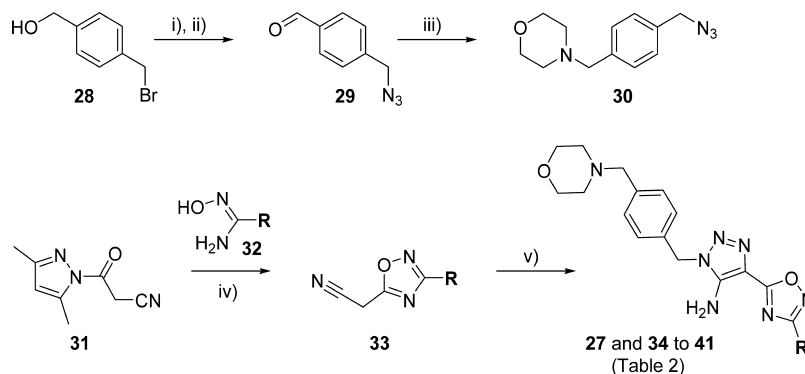
for release in vivo of 3-methoxy aniline, which is known to be a potent mutagen and carcinogen.<sup>49</sup>

Although there was some evidence for hydrolysis of **11**, there was no evidence for release of 3-methoxyaniline from **20** after oral dosing in mouse or after incubation in mouse plasma at 37 °C for 5 h. However, it was thought prudent to identify an improved lead which negated the mutagenesis risk associated with undetected release of the aniline in vivo. It was also recognized that the aniline makes an important contribution to binding because truncation of the aniline of **11** to the simple primary amide (CONH<sub>2</sub>, **S39**) abolished activity (see Supporting Information, Table S5). Two complementary strategies were therefore adopted primarily focused upon mitigation of the Ames risk; identifying bioisosteres of the amide bond which could not be hydrolyzed to give an aniline and identification of Ames negative anilines which retained activity. Improvement of the hERG safety margin was also sought by attempting to modulate the lipophilicity of the benzamide portion of the molecule.

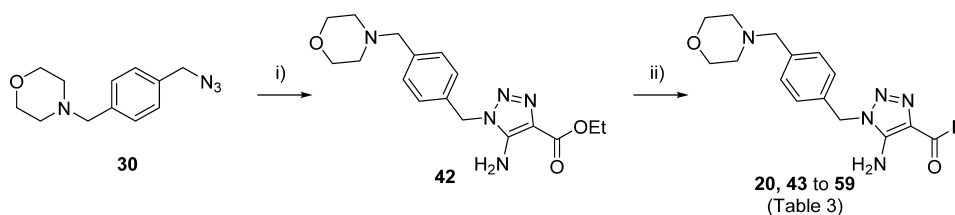
**Evaluation of Amide Bioisosteres.** Compound **11** was initially used as a synthetically convenient template to explore amide replacements. Classical topological-based isosteric replacements of the amide functionality,<sup>50</sup> such as sulphone (**S40**), ketone (**S41**), and hydroxyethyl (**S42**) (see Supporting Information, Table S5), were not effective surrogates of the parent amide in this system. However, replacement with biaryl and fused bicyclic heterocycles which retained a HBA in place

of the amide oxygen possessed promising activity, with pEC<sub>50</sub> > 6.0 (see Supporting Information, Table S5 and Scheme S4 for details of synthesis and activity of these). Investigation of the effect of substitution on the phenyl ring of oxadiazole **S44** (see Supporting Information, Table S5) showed that *ortho* substitution gave a 5-fold improvement in potency compared to no substituent, whereas no improvement in potency was observed for *meta* substituted analogue (i.e., **S45** and **S46** see Supporting Information, Table S5).

Oxadiazole **27** was ultimately identified as the most promising bioisostere of the amide bond on the basis of its activity and PFI. Although this modification largely retained the activity of **20** and effectively discharged the risk associated with in vivo release of a mutagenic aniline, compound **27** had much lower metabolic stability when incubated with mouse liver microsomes, prompting examination of additional modifications to the oxadiazole substituent which might address this (see Table 2). A variety of different analogues were prepared in which a mimic or replacement of the 3-methoxyphenyl group of compound **11** were investigated. This included aromatic rings with a methoxy substituent, heteroaromatics (five-membered and six-membered) and aliphatics (Table 2 and Supporting Information, Table S6). Compound **27** and analogues **34**–**41** were synthesized by base-promoted cyclization of a substituted oxadiazolyl acetonitrile **33** with 4-(4-(azidomethyl)benzyl)morpholine **30** (Scheme 2). Azide **30** could be prepared in three steps from commercially available

Scheme 2. Synthesis of Oxadiazole 27 and Analogues in Table 2<sup>a</sup>

<sup>a</sup>Reagents: (i)  $\text{NaN}_3$ , DMF; (ii)  $\text{MnO}_2$ , DCM; (iii) morpholine,  $\text{NaB}(\text{OAc})_3\text{H}$ ,  $\text{CHCl}_3$ ; (iv) *N*-hydroxyamide, 1,4-dioxane; (v) NaOMe, MeOH, then add azide 30.

Scheme 3. Synthesis of Amides in Table 3<sup>a</sup>

<sup>a</sup>Reagents: (i) ethylcyanoacetate, NaOEt, EtOH; (ii) amine “RH” (see Table 3),  $\text{AlMe}_3$ , toluene.

(4-(bromomethyl)phenyl)methanol 28 (see Scheme 2), and acetonitrile intermediates 33 were prepared in one step by condensation of 3-(3,5-dimethyl-1*H*-pyrazol-1-yl)-3-oxopropanenitrile 31 with the appropriate amidoxime 32.

The addition of a methoxy group intended to mimic that of 20 (i.e., 34), improved activity and reduced binding to hERG ( $>30 \mu\text{M}$ ), but metabolic stability was not improved. Metabolic stability could be significantly improved through reductions in PFI, i.e., by replacing the oxadiazole phenyl with various cyclic ethers or hydroxylated cycloalkyl groups (i.e., 35 and 36, see Supporting Information, Table S6 for further examples), although these compounds were unfortunately inactive. Compounds where the methoxyphenyl ring was replaced with a 2-methoxy-substituted heterocycle generally had better metabolic stability (i.e., 37, 38, 39, 40), although only compound 37 offered improved potency combined with good metabolic stability. Moreover, because hERG inhibition was also low ( $\text{IC}_{50} > 30 \mu\text{M}$ ), this compound represented the best lead from this series.

**Identification of an Alternative Amide Derived from an Ames Negative Amine.** Alternative amines to 3-methoxy aniline were also examined as a complementary strategy for addressing the *pro*-mutagenic potential of 20. There are several factors involved in activation of an aromatic amine to the actual DNA-reactive nitrenium species, structure–mutagenicity relationships are poorly understood, and there is a paucity of literature information on the Ames status of amines. Therefore, because amides could be conveniently prepared by direct substitution of ethyl ester 42 with an amine under Lewis acid conditions ( $\text{AlMe}_3$ ), a prospective approach was adopted using parallel synthesis to identifying suitable alternatives (see Scheme 3). A diverse library of amides was prepared and evaluated, excluding amines known to be Ames positive. For final compounds showing good potency and FaSSIF solubility, a high

priority was conducting an Ames test on the constituent amine unless they were already reported as Ames negative.

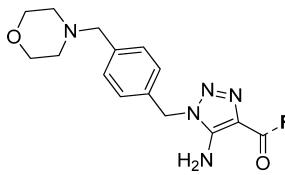
Only directly linked aromatic or heteroaromatic amides had the desired level of activity (i.e.,  $\text{pEC}_{50} > 6$ ). Benzylic compounds were inactive (i.e., compare *N*-benzyl analogue 44 with *N*-phenyl compound 43, Table 3). The most active nonaromatic system was the adamantyl amide 45 ( $\text{pEC}_{50} = 5.5$ ), while all others were substantially inactive, including the closest fully saturated analogue of 20 (i.e., 46). *N*-Methylation of the amide, which is known to improve the hydrolytic resistance of aniline amides such as phenacetin,<sup>51</sup> in this case resulted in significantly reduced activity (i.e., compare 47 with 20).

The *meta*-methoxy of 20 could be replaced with a variety of alternative groups including  $-\text{OCF}_3$  (S70),  $\text{CF}_3$  (S71), acetylene (S72) (see Supporting Information, Table S7), and chloro (48) while retaining activity and solubility, but of these only the former had marginally better metabolic stability than the benchmark compound 20. 3-Methyl (49) and 3-fluoro analogues (50) were of similar potency to 20, and highly selective, but they did not offer an advantage with respect to metabolic stability. Conversely, anilides with substantially more polar groups in the *meta*-position (for example  $\text{CH}_2\text{NMe}_2$  (S73),  $\text{SO}_2\text{Me}$  (S74), and amide (S75) (see Supporting Information, Table S7) were at least 100-fold less active.

Although there is evidence to suggest heteroaromatic amines have a reduced risk of being mutagenic<sup>52</sup> and that increases in polarity can also reduce hERG inhibition,<sup>53</sup> it was unfortunate that pyridine or pyrimidine analogues of 20 had lower activity (i.e., 51, 52, and 53) and were not considered as suitable leads.

Applying an inductive ( $-I$ ) effect by addition of fluorine atoms at various positions of the *meta*-methoxy anilide of 20 would be considered a logical approach to reducing Ames risk because electron density of the parent arylamine is one

Table 3. Optimization of the Amide Substituent



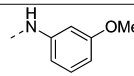
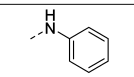
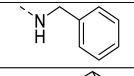
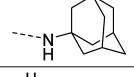
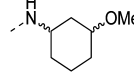
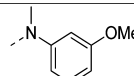
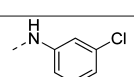
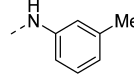
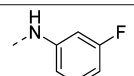
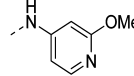
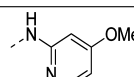
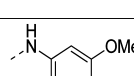
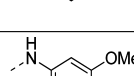
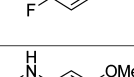
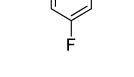
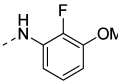
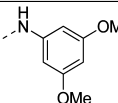
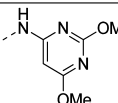
R	Compound	T.cruzi pEC <sub>50</sub>	VERO pEC <sub>50</sub>	Cl <sub>50</sub> <sup>b</sup> (mouse)	Solubility <sup>c</sup> (μM)	Chi LogD (PFI)	hERG (μM)	FaSSIF (μg/mL)
	<b>20</b>	7.0	< 4.3	3.6	> 250 (219) <sup>d</sup>	2.2 (7.0)	24	264
	<b>43</b>	5.9	4.49	2.1	> 250 <sup>d</sup>	2.0 (6.8)	nd	nd
	<b>44</b>	< 4.3	< 4.3	10.6	219	nd	nd	nd
	<b>45</b>	5.5	4.34	nd	> 250	3.4 (7.9)	nd	nd
	<b>46</b>	< 4.3	< 4.3	nd	> 250	1.4 (4.7)	nd	nd
	<b>47</b>	< 4.3	< 4.3	3.5	> 250 <sup>d</sup>	2.6 (7.6)	nd	nd
	<b>48</b>	7.8	4.51	3.7	> 250 <sup>d</sup>	2.3 (7.2)	18	38
	<b>49</b>	7.0	< 4.3	4.1	> 250 <sup>d</sup>	2.4 (7.3)	nd	27
	<b>50</b>	6.9	< 4.3	4.3	> 250 <sup>d</sup>	2.3 (7.15)	7	27
	<b>51</b>	6.7	< 4.3	2.1	> 250 <sup>d</sup>	2.1 (7.6)	> 100	24
	<b>52</b>	6.6	< 4.3	33	> 250	0.3 (3.8)	nd	nd
	<b>53</b>	6.5	< 4.3	2.2	> 250 <sup>d</sup>	nd	5	898
	<b>54</b>	7.7	< 4.3	3.7	> 250 <sup>d</sup>	2.4 (7.1)	36	39
	<b>55</b>	7.7	< 4.3	6.3	> 250 <sup>d</sup>	2.4 (7.3)	nd	61
	<b>56</b>	6.1	< 4.3	2.5	> 250 <sup>d</sup>	2.1 (6.8)	nd	nd



Table 3. continued

R	Compound	<i>T. cruzi</i> pEC <sub>50</sub>	VERO pEC <sub>50</sub>	Cl <sub>i</sub> <sup>b</sup> (mouse)	Solubility <sup>c</sup> (μM)	Chi LogD (PFI)	hERG (μM)	FaSSIF (μg/mL)
	57	5.5	< 4.3	3.5	> 250 <sup>d</sup>	2.1 (6.8)	nd	nd
	58	7.1	< 4.3	4.7	> 250 <sup>d</sup>	2.2 (7.0)	23	577
	59	7.4	< 4.3	3.4	> 250 <sup>d</sup>	2.1 (6.9)	113	100

<sup>a</sup>pEC<sub>50</sub> values are shown as mean values from two or more EC<sub>50</sub> determinations. Standard deviation is typically within 2-fold from the EC<sub>50</sub>. <sup>b</sup>Cl<sub>i</sub> when incubated with liver microsomes; mL min<sup>-1</sup> g<sup>-1</sup>. <sup>c</sup>Kinetic aqueous solubility at pH 7.4 measured by nephelometry. <sup>d</sup>Kinetic aqueous solubility at pH 7.4 measured by nephelometry of the HCl salt.

Table 4. Comparison of the Activity and Pharmacokinetic Profile of Optimized Amides 48, 58, 59, and Oxadiazole 37 with Early Leads 11 and 20

compd	<i>T. cruzi</i> pEC <sub>50</sub>	VERO pEC <sub>50</sub>	mouse Cl <sub>i</sub> <sup>a</sup>	mouse PPB (% bound)	hERG IC <sub>50</sub> (μM)	AUC (0–8 h) (ng·min/mL)	C <sub>max</sub> (ng/mL)	PFI	FaSSIF (μg/mL)	CYP-3A4 pEC <sub>50</sub>
11	7.4	<4.3	3.2	nd	nd	3200	17	8.9	nd	nd
20	7.0	<4.3	3.6	80	24	260000	1300	7.0	264 <sup>b</sup>	<4.4
48	7.8	4.5	3.7	88	17	250000	710	7.2	38	<4.4
58	7.1	<4.3	4.7	93	23	370000	1600	7.0	577 <sup>b</sup>	<4.4
59	7.4	<4.3	3.4	69	113	300000	1300	6.8	100 <sup>b</sup>	<4.4
37	7.1	<4.3	3.3	66	>30	190000	1300	7.2	18 <sup>b</sup>	<4.4

<sup>a</sup>Cl<sub>i</sub> when incubated with liver microsomes; mL min<sup>-1</sup> g<sup>-1</sup>. <sup>b</sup>Solubility in simulated fasted intestinal fluid (FaSSIF) was determined on the monohydrochloride salts.

recognized factor influencing bioactivation by aromatic oxidation.<sup>54</sup> Surprisingly, potency was very sensitive to the position of fluorination; while a fluorine atom either *meta*- or *para*- to the methoxy actually improved activity by 7-fold (55 and 54), fluorine in the *ortho*- position reduced activity by more than 10-fold (56 and 57). A similar trend was observed in difluoro analogues (see Supporting Information, Table S7), which were all significantly less potent than 20. Given that additional functionalities *meta*- to the methoxy could enhance potency, it was found that addition of a 5-methoxy (i.e., 58) improved activity without detriment to metabolic stability and selectivity. This 3,5-dimethoxy arrangement was also significantly active in a pyrimidine system (59). The constituent amines of amides 48, 58, and 59 (i.e., 3-chloroaniline, 3,5-dimethoxy aniline, and 2,6-dimethoxypyrimidin-4-amine) as well as parent compounds (58 and 59 only) were shown to be Ames-negative in the presence or absence of rat liver S9 fraction. On the basis of having high potency (pEC<sub>50</sub> > 7), selectivity against VERO cells (>100-fold), hERG (>30 μM), and having resolved the Ames liability, the amides 48, 58, and 59 and the oxadiazole 37 were selected for further profiling.

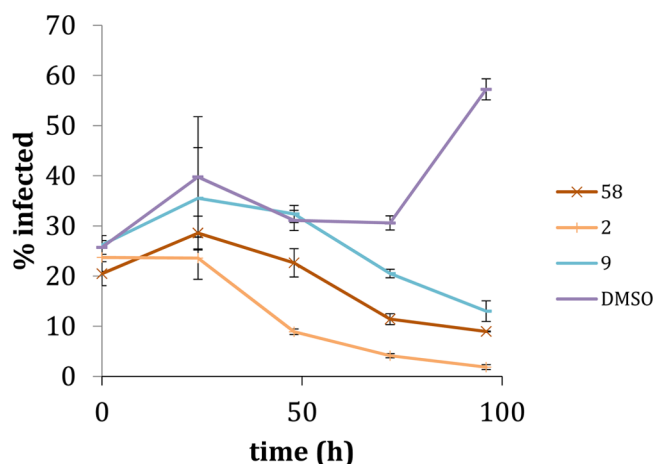
## CELL BIOLOGY AND PHARMACOLOGY OF THE ATC SERIES

Pharmacokinetic parameters for 20, 37, 48, 58, and 59 were determined in female NMRI mouse following a single 10 mg/kg oral dose (see Table 4 and Supporting Information,

Figures S8–S12). These were selected as the most promising examples of the various series, in terms of potency, selectivity, metabolic stability, and solubility. All compounds had oral exposure that was significantly improved compared to that of early lead compound 11, presumably as a consequence of improved solubility.

The ability of compounds from this series to kill parasites rather than merely inhibiting their replication was confirmed using a static-cidal assay on the intracellular amastigote form of the parasite.<sup>22</sup> The “rate of kill” of *T. cruzi* intracellular parasites was also measured and compared to nifurtimox (2) (which has a very rapid onset (0–24 h) of parasite killing) and posaconazole (9) (which has a slower lag (24–48 h) before killing occurs (Figure 3)). The rate of kill of ATC series compounds 11, 20, 48, 58, 59 (amides), and 37 (oxadiazole) was slower than nifurtimox. With nifurtimox, parasite growth stopped immediately and decreased rapidly after 24 h. However, with compound 58, parasite growth continued for 24 h before starting to decrease. Compound 58 gave a comparable rate of kill to posaconazole, a potent inhibitor of the important sterol biosynthesis enzyme of *T. cruzi*, lanosterol-14 $\alpha$ -demethylase<sup>55</sup> (*TcCYP-51*).

Our high throughput screening efforts have revealed a relatively high proportion of hit series whose apparent target is *TcCYP-51*. This is a mode of action which needed to be deprioritized, given the recent disappointing phase 2 clinical trial results with *TcCYP51* inhibitors posaconazole and E1224



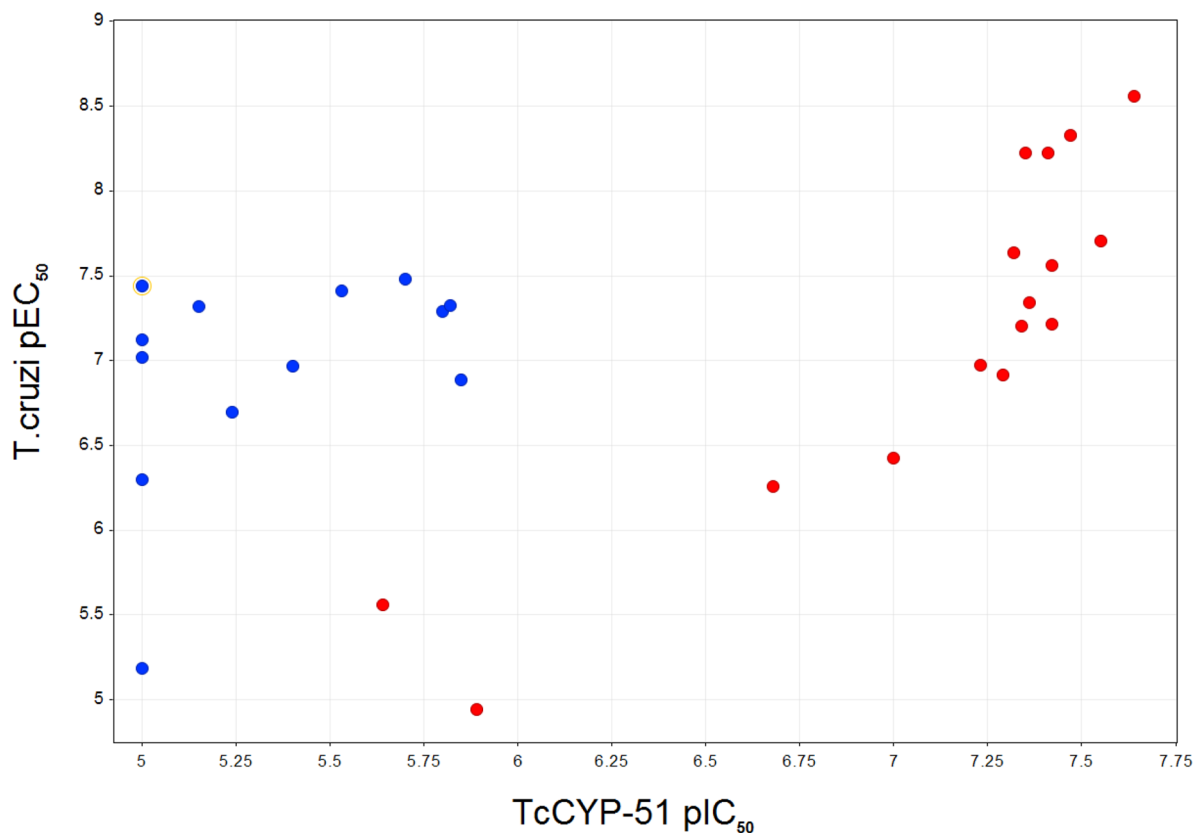
**Figure 3.** Rate of kill of compound 58 compared to nifurtimox (2) (fast kill) and posaconazole (9) (slow-kill).

(the phosphate prodrug of ravuconazole)<sup>18,19</sup> and the significant number of series against this target currently being developed.<sup>56–61</sup> It is unlikely, however, that the mode of action of the ATC series is via *TcCYP-51* because, in spite of containing a common CYP inhibitor motif (the 1,2,3-triazole ring), trypanocidal activity does not correlate with *TcCYP-51* enzyme inhibition (see Figure 4) measured using a *TcCYP51* inhibition assay.<sup>62</sup> Nevertheless, there remains the remote possibility that this series is exerting activity through mechanism-based inhibition<sup>63</sup> of *TcCYP-51*, i.e., via bioactivation to a suicide substrate, and time-dependency has not been investigated to rule this out.

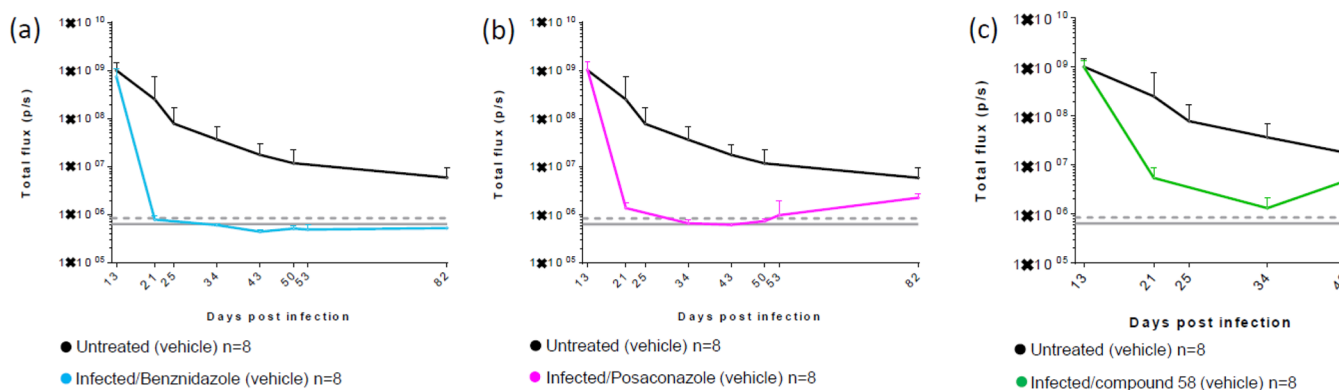
*T. cruzi* is a genetically diverse parasite which has been assigned six discrete typing units (DTU). It is important to consider strain diversity<sup>64</sup> to ensure compounds from any given series are not just active against the Silvio X10/7 clone A1 (DTU Tc1) strain used in routine screening. Thus, it was confirmed that representative compounds 20, 58, 48, and 59 all showed activity of  $pEC_{50} > 6$  against a panel of key *T. cruzi* discrete typing units including YUAM, M6241 Clone 6, Era Clone 2, and Tula Clone 2 (DTU Tc II, III, IV, and VI, respectively). However, the slow-growing PAH179 Clone 5 (Tc V) strain was significantly less sensitive to compounds from this series (data not shown).

A representative set of compounds from this series was also tested against *Leishmania donovani*, *Trypanosoma brucei*, and *Plasmodium falciparum* parasites in standard assays and were found to be essentially inactive ( $pEC_{50} < 5.0$ ).

**Efficacy in Acute and Chronic Mouse Models of Chagas' Disease.** There are several mouse models of Chagas' disease currently being used, although it is not clear which of these will be better at predicting clinical success, given the lack of clinically effective compounds to back-translate. Consequently, a BALB/c mouse model of acute and chronic Chagas' disease was chosen that could at least reproduce posaconazole (9) and benznidazole (1) clinical outcome. This model uses *T. cruzi* (clone CL Brener), which express a red-shifted luciferase reporter that emits tissue-penetrating orange-red light when luciferin is injected.<sup>65</sup> Compound 58 was selected for further evaluation in this model (acute and chronic) as an exemplar of the series to establish proof-of-concept. This compound had the best total exposure and significantly better FaSSIF solubility

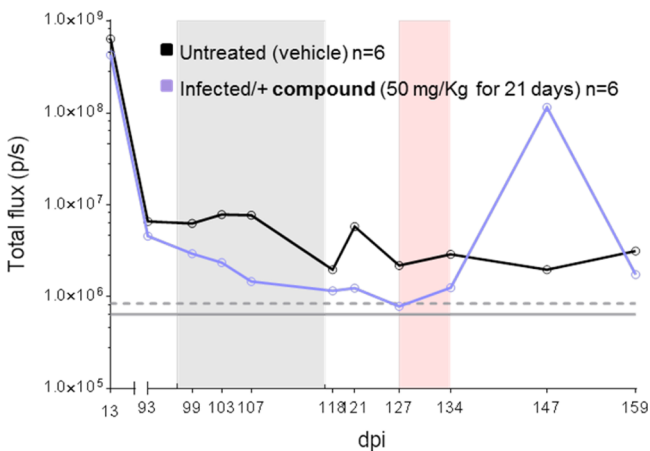


**Figure 4.** Relationship between parasite activity (*T. cruzi*  $pEC_{50}$ ) and inhibition of the *TcCYP-51* enzyme for compounds in the ATC series (blue) compared to a training set of known antifungal azole CYP-51 inhibitors (red) (see Supporting Information, Table S8 for structures and  $IC_{50}$  data).



**Figure 5.** Parasite load, as determined by bioluminescent imaging, in the acute mouse model.<sup>65</sup> (a) Benznidazole (**1**) dosed at 100 mg/kg u.i.d. for 21 days. (b) Posaconazole (**9**) at 20 mg/kg u.i.d. for 20 days. (c) **58** dosed at 50 mg/kg b.i.d. for 21 days. Vehicle control is shown as red line.

and relatively similar potency compared to alternative compounds profiled in detail, such as compound **59** (Table 4). When **58** was evaluated (50 mg/kg b.i.d. orally for 20 days), against both the acute (treatment initiated 14 days post-infection) and chronic stages (97 days post-infection) of the infection, sterile cure, as seen for benznidazole (**1**), was not achieved. In both the acute and chronic models with **58**, the parasite burden was considerably reduced but not eliminated (Figures 5–7). Following the “chronic” experiment, ex vivo imaging indicated that most of the parasites were found in the colon (Figure 7).



**Figure 6.** Parasite load, as determined by bioluminescent imaging, in the chronic mouse model<sup>65</sup> following treatment with **58** at 50 mg/kg b.i.d. for 21 days (gray shaded area) compared to vehicle control. Parasite rebound was observed at day 147 following immune suppression with cyclophosphamide (pink shaded area) (Experimental Section).

Bioanalysis of spot blood sampling from the infected animals in each study demonstrated that blood-free levels of **58** were maintained at least  $2 \times EC_{90}$  for the duration of dosing (21 days b.i.d.), once a correction for plasma protein binding had been applied.

## CONCLUSIONS

In this paper, the discovery and optimization of a novel compound series is described which demonstrates potent activity against the *T. cruzi* parasite and parasite knockdown in murine models of acute and chronic Chagas’ disease following oral

dosing. A summary of structure–activity findings are shown in Figure 8.

We have shown that significant issues with this series, i.e., poor oral exposure, hERG activity, and potential mutagenicity could be addressed to obtain compounds with an improved safety profile suitable for evaluation in a murine model of Chagas’ disease. Compounds **58** and **59** were the most promising in terms of potency, PFI, oral exposure (AUC), FaSSIF solubility, and hERG.

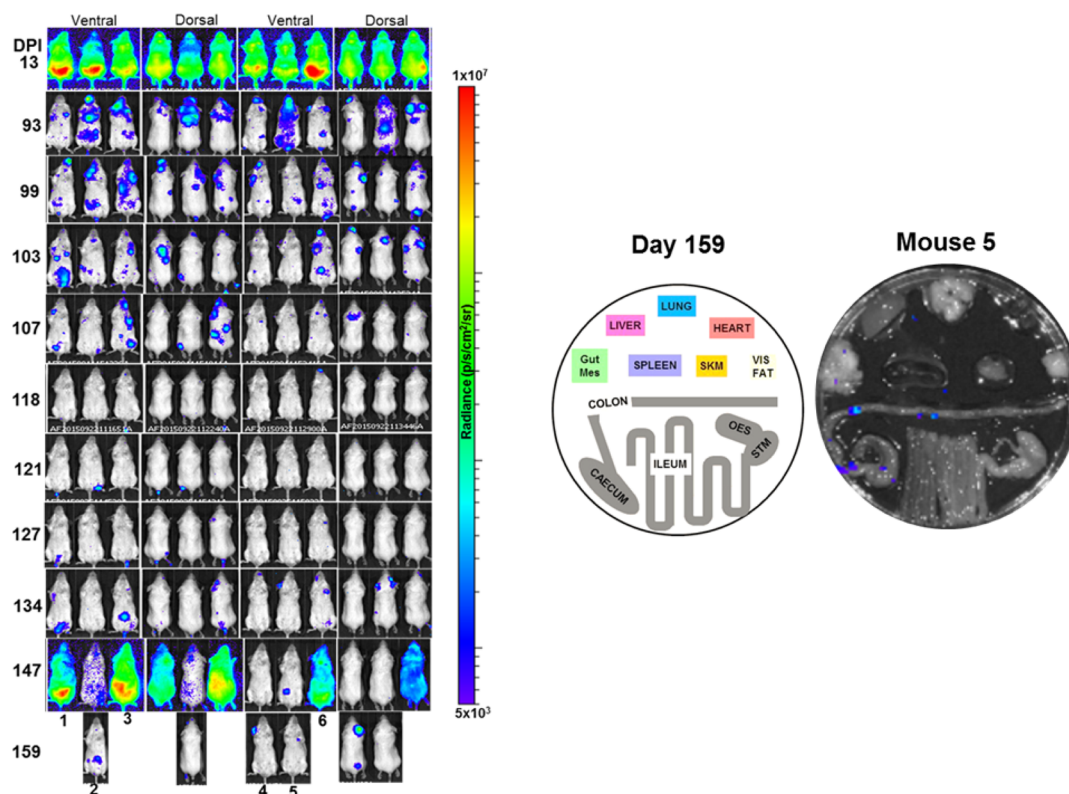
This compound series appears to have a different molecular mode of action to posaconazole. However, it showed a similar rate of kill against the parasites as posaconazole (Figure 3). In addition, as for posaconazole, it showed significantly reduced activity against a slow growing strain of *T. cruzi*. There is currently no evidence that rate of kill correlates with in vivo activity, in particular as dosing in the in vivo efficacy studies is much longer than the 4 days used in the rate of kill experiment. However, by comparing such data across different chemical series, it may be possible to determine which in vitro experiments are predictive of in vivo efficacy. Hence, we thought it is important to share this data with others working in the field.

This compound series demonstrated significant reduction of parasite burden in mouse models of acute and chronic Chagas’ disease but was unable to deliver sterile cures under the conditions used. Current focus is on trying to understand the reasons for this: whether it is driven by pharmacokinetic (tissue distribution) or mechanistic considerations. It is possible that the slow rate of kill of the compound against the parasite and the reduced activity against slow growing strains of *T. cruzi* may be predictive of a noncurative in vivo outcome. This needs further investigation.

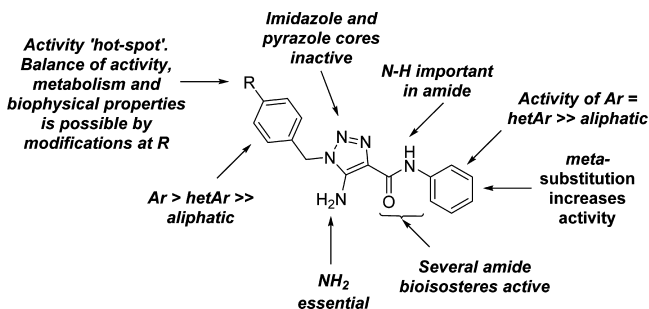
While this compound series itself is not progressible toward the clinic, it is providing valuable learnings in our ultimate goal of developing new medicines for Chagas’ disease.

## EXPERIMENTAL SECTION

**General Experimental Information.** Chemicals and solvents were purchased from the Aldrich Chemical Co., Fluka, ABCR, VWR, Acros, Fisher Chemicals, and Alfa Aesar and were used as received unless otherwise stated. Air- and moisture-sensitive reactions were carried out under an inert atmosphere of argon in oven-dried glassware. Analytical thin-layer chromatography (TLC) was performed on precoated TLC plates (layer 0.20 mm silica gel 60 with fluorescent indicator UV254, from Merck). Developed plates were air-dried and analyzed under a UV lamp (UV254/365 nm). Flash column chromatography was performed using prepacked silica gel cartridges



**Figure 7.** Time-course bioluminescence ventral and dorsal images of mice ( $n = 6$ ) treated with compound **58** (50 mg/kg b.i.d; 21 days) in the chronic model (left). Ex-vivo imaging of organs from mouse 5 at the end of the experiment (day 159; right) indicates that the residual parasites were localized primarily in the colon.



**Figure 8.** Summary of the structure–activity relationships for the ATC series.

(230–400 mesh, 40–63  $\mu\text{m}$ , from SiliCycle) using a Teledyne ISCO Combiflash Companion or Combiflash Retrieve.  $^1\text{H}$  NMR,  $^{13}\text{C}$  NMR,  $^{19}\text{F}$  NMR, and 2D NMR spectra were recorded on a Bruker Avance DPX 500 spectrometer ( $^1\text{H}$  at 500.1 MHz,  $^{13}\text{C}$  at 125.8 MHz,  $^{19}\text{F}$  at 470.5 MHz). Chemical shifts ( $\delta$ ) are expressed in ppm recorded using the residual solvent as the internal reference in all cases. Signal splitting patterns are described as singlet (s), doublet (d), triplet (t), quartet (q), multiplet (m), broad (b), or a combination thereof. Coupling constants ( $J$ ) are quoted to the nearest 0.1 Hz. LC-MS analyses were performed with either an Agilent HPLC 1100 series connected to a Bruker Daltonics MicrOTOF or an Agilent Technologies 1200 series HPLC connected to an Agilent Technologies 6130 quadrupole LC/MS, where both instruments were connected to an Agilent diode array detector. All assay compounds had a measured purity of  $\geq 95\%$  as determined using this analytical LC-MS system (TIC and UV). High resolution electrospray measurements were performed on a Bruker Daltonics MicrOTOF mass spectrometer. Microwave-assisted chemistry was performed using a Biotage Initiator microwave synthesizer. Purity ( $>97\%$ ) and molecular mass were confirmed by HPLC and high resolution mass spectrometry.

**Prototypical Procedure for the Cyclization Reaction between an  $\alpha$ -Cyanoacetic Ester or Amide with an Azide Formed in Situ: Preparation of 5-Amino-N-(3-methoxyphenyl)-1-[(4-pyrazol-1-ylphenyl)methyl]triazole-4-carboxamide (14).** Sodium azide (253 mg, 3.89 mmol) was added to a stirred solution of 1-[4-(chloromethyl)phenyl]pyrazole (250 mg, 1.30 mmol) in DMF (8.0 mL) at rt, then the slurry was warmed to 80  $^\circ\text{C}$  for 1 h. The reaction was then concentrated in vacuo, the residue partitioned between water (10 mL) and EtOAc (10 mL), and the organic phase separated, dried ( $\text{MgSO}_4$ ), and concentrated. The residual oil was then immediately dissolved in EtOH (8.0 mL), 2-cyano-N-(3-methoxyphenyl)acetamide (250 mg, 1.30 mmol) added, followed by finely ground sodium hydroxide (52 mg, 1.30 mmol), and the reaction heated to 80  $^\circ\text{C}$  for 1 h in the microwave. The cooled reaction was then concentrated in vacuo, the residue partitioned between 1 M HCl (25 mL) and EtOAc (25 mL), the organic phase separated, dried ( $\text{MgSO}_4$ ), and concentrated in vacuo to give a residue, which was triturated from EtOAc, collected by filtration, and dried under vacuum to give the title compound as a white powder (285 mg, 0.73 mmol, 56%).  $^1\text{H}$  NMR (500 MHz,  $\text{DMSO}-d_6$ ):  $\delta$  10.03, (s, 1H), 8.48 (s, 1H), 7.85 (d,  $J = 8.3$  Hz, 2H), 7.75 (d,  $J = 1.0$  Hz, 1H), 7.56 (t,  $J = 1.9$  Hz, 1H), 7.42 (d,  $J = 7.8$  Hz, 1H), 7.37 (d,  $J = 8.3$  Hz, 2H), 7.20 (t,  $J = 8.6$  Hz, 1H), 6.68 (s, 2H), 6.63 (dd,  $J = 2.1$  Hz, 8.2 Hz, 1H), 6.55 (t,  $J = 2.0$  Hz, 1H), 5.51 (s, 2H), 3.73 (s, 3H). HRMS ( $m/z$ ):  $[M + H]^+$  calcd for  $\text{C}_{20}\text{H}_{20}\text{N}_7\text{O}_2$ , 390.1673; found, 390.1666.

**4-[[4-(Azidomethyl)phenyl]methyl]morpholine (30).** Sodium azide (14.5 g, 223.5 mmol) was added portionwise into a solution of [4-(chloromethyl)phenyl]methanol (25.0 g, 159.6 mmol) in DMF (800 mL) at rt, and the reaction was then warmed to 60  $^\circ\text{C}$  behind a blast shield for 3 d. The reaction mixture was then allowed to cool to rt then concentrated in vacuo at minimum pressure behind a blast shield with water bath temperature of  $<60$   $^\circ\text{C}$ . The residual oil was then diluted with brine (300 mL) and  $\text{Et}_2\text{O}$  (600 mL), and the organic phase separated, washed with brine ( $3 \times 100$  mL), dried ( $\text{MgSO}_4$ ), and concentrated in vacuo to give 27.9 g of crude azide as a colorless

oil. This was then taken up into DCM (750 mL) at rt, and MnO<sub>2</sub> (50.0 g, 574.7 mmol) added portionwise. The slurry was stirred at 40 °C for 48 h before filtration through a pad of Celite. The filtrate was concentrated in vacuo to give 23.9 g of a colorless oil, which was a single component on TLC. The oil was then immediately taken up into chloroform (1000 mL) and treated with morpholine (25.8 g, 296.1 mmol), 20 g of 4 Å molecular sieves were added, and the solution was stirred at 40 °C for 2 h prior to removal of the sieves by filtration. The solution was then cooled to 0 °C and treated portionwise with sodium triacetoxyborohydride (50.0 g, 235.9 mmol) with careful monitoring of the temperature, such that it did not rise above 5 °C. After 3 h, the reaction was allowed to warm to room temperature prior to warming to 45 °C for 48 h. The reaction was then quenched by careful addition of 2N NaOH (aq) (250 mL) with stirring, the organic phase separated, and the aqueous phase extracted with chloroform (3 × 100 mL). The combined extracts were dried (MgSO<sub>4</sub>), filtered, and concentrated in vacuo to give a clear oil which contained desired product contaminated with approximately 10% *N*-acetyl morpholine as impurity. Chromatography (SiO<sub>2</sub>, 330 g prepacked column eluting with EtOAc) allowed straightforward separation to give the title compound as a colorless oil (28.6 g, 120.7 mmol, 76% overall yield for 3 steps), which was stored at -18 °C. <sup>1</sup>H NMR (500 MHz, DMSO-*d*<sub>6</sub>): δ 7.38 (d, *J* = 8.0 Hz, 2H), 7.30 (d, *J* = 8.4 Hz, 2H), 4.35 (s, 2H), 3.75–3.72 (t, *J* = 4.6 Hz, 4H), 3.53 (s, 2H), 2.47 (t, *J* = 4.6 Hz, 4H).

**Caution:** Some azides are known to be explosive. Thermal hazard screening was carried out on azide **30**. Differential scanning calorimetry indicated that the temperature at which heat flow exceeds 0.01 W/g = 180 °C. Simple impact test was negative, hot plate tests were inconclusive, and oxygen balance test deemed the compound to be low risk. Further tests should be considered if the proposed processing or drying temperature is above 80 °C.

**Ethyl 5-Amino-1-(4-(morpholinomethyl)benzyl)-1H-1,2,3-triazole-4-carboxylate (42).** A stirred solution of sodium ethoxide (6.45 g, 94.71 mmol) in EtOH (100 mL) at 0 °C was treated dropwise with ethyl 2-cyanoacetate (9.74 g, 86.10 mmol). After 10 min, a solution of 4-[[4-(azidomethyl)phenyl]methyl]morpholine (10.0 g, 43.05 mmol) in EtOH (20 mL) was added dropwise, then the reaction was allowed to warm to rt before being heated to reflux for 3 h. After cooling to rt, the reaction was diluted by addition of water (200 mL) and EtOAc (200 mL), the organic phase was separated, the aqueous layer was extracted with EtOAc (3 × 50 mL), and the combined extracts were dried (MgSO<sub>4</sub>) and concentrated in vacuo to give a residual solid which was triturated with Et<sub>2</sub>O, collected by filtration, and dried in vacuo to give the title compound (7.20 g, 20.64 mmol, 48%) as a white powder. <sup>1</sup>H NMR (500 MHz, DMSO-*d*<sub>6</sub>): δ 7.29 (d, *J* = 8.0 Hz, 2H), 7.17 (d, *J* = 8.0 Hz, 2H), 6.57 (s, 2H), 5.42 (s, 2H), 4.26 (q, *J* = 7.1 Hz, 2H), 3.55 (t, *J* = 4.6 Hz, 4H), 3.43 (s, 2H), 2.32 (t, *J* = 4.2 Hz, 4H), 1.29 (t, *J* = 7.1 Hz, 3H). *m/z* (ES<sup>+</sup>, 70 V) 346.1 [MH<sup>+</sup>].

**Prototypical Procedure for the Lewis-Acid Catalyzed Direct Amidation of an Ester with an Amine: Preparation of 5-Amino-*N*-(3,5-dimethoxyphenyl)-1-[[4-(morpholinomethyl)phenyl]methyl]triazole-4-carboxamide Hydrochloride (58).** To a well stirred suspension of ethyl 5-amino-1-[[4-(morpholinomethyl)phenyl]methyl]triazole-4-carboxylate (3.0 g, 8.60 mmol) and 3,5-dimethoxyaniline (2.66 g, 17.37 mmol) in toluene (250 mL) at rt was added trimethylaluminum (2 M in toluene, 10.0 mL, 20.0 mmol). Fuming on addition of the trimethylaluminum was noted. The reaction mixture was then heated to 80 °C for 18 h with periodic monitoring by LCMS and tlc (the reaction gradually became a solution). The reaction was then cooled to rt, quenched carefully by slow addition of 2N NaOH (aq) (150 mL) and the ensuing biphasic mixture extracted with EtOAc (3 × 50 mL), allowing 10–20 min for each separation due to turbidity. The organic phase was washed with brine (100 mL), then saturated aqueous Rochelle's salt (100 mL), dried (MgSO<sub>4</sub>), filtered, and concentrated in vacuo. The resulting oil was taken up into 100 mL of 1:1 EtOAc/Et<sub>2</sub>O and stirred at rt for 3 days, during which time a precipitate was formed. Filtration and copious washing with cold diethyl ether gave 3.26 g of the free base. This was then taken up into

Et<sub>2</sub>O (100 mL) and treated dropwise with 2 M HCl in Et<sub>2</sub>O (7.0 mL) and the slurry stirred at rt for 18 h prior to collection by filtration under a nitrogen atmosphere and washing with Et<sub>2</sub>O to give the title compound as an off-white powder (3.45 g, 6.70 mmol, 77%). <sup>1</sup>H NMR (500 MHz, DMSO-*d*<sub>6</sub>): δ 9.77 (s, 1H), 7.65 (d, *J* = 8.2 Hz, 2H), 7.34 (d, *J* = 8.2 Hz, 2H), 7.14 (d, *J* = 7.3 Hz, 2H), 6.89 (s, br, 2H), 6.22 (t, *J* = 7.3 Hz, 1H), 5.54 (s, 2H), 4.31 (s, 2H), 3.96–3.74 (m, 4H), 3.73 (s, 6H), 3.23–3.16 (m, 2H), 3.11–3.01 (m, 2H). HRMS (*m/z*): [M + H]<sup>+</sup> calcd for C<sub>23</sub>H<sub>28</sub>N<sub>6</sub>O<sub>4</sub>, 453.2245; found, 453.2263.

**Prototypical Procedure for Formation of an Azide from an Amine with 1*H*-Imidazole-1-sulfonyl Azide Hydrochloride: Preparation of 2-Azido-2-(4-isopropylphenyl)ethanol (60), Used in the Synthesis of 24.** 1*H*-Imidazole-1-sulfonyl azide hydrochloride (1.54 g, 8.93 mmol) was added portionwise to a well-stirred slurry of 2-amino-2-(4-isopropylphenyl)ethanol (1.0 g, 5.58 mmol) and potassium carbonate (1.54 g, 11.16 mmol) in MeOH (10.0 mL) at rt and the reaction left for 18 h. The mixture was then concentrated in vacuo, partitioned between DCM (25 mL) and water (25 mL), the organic phase separated, dried (MgSO<sub>4</sub>), and concentrated to give a yellow oil which was purified by flash column chromatography (SiO<sub>2</sub>, 1:10 to 1:1 EtOAc:hexanes) to give the title compound as a clear oil (435 mg, 2.12 mmol, 38%). <sup>1</sup>H NMR (500 MHz, CDCl<sub>3</sub>): δ 7.48 (s, 4H), 4.67 (t, *J* = 6.5 Hz, 1H), 3.77 (dd, *J* = 5.9 Hz, 5.9 Hz, 2H), 2.98–2.91 (m, 1H), 1.97 (dd, *J* = 5.8 Hz, 5.8 Hz, 1H), 1.28 (d, *J* = 6.9 Hz, 6H).

**2-Cyano-*N*-(3-methoxyphenyl)acetamide (61).** A slurry of 3-(3,5-dimethylpyrazol-1-yl)-3-oxo-propanenitrile (5.0 g, 30.6 mmol) suspended in toluene (50 mL) was treated with 3-methoxyaniline (3.77 g, 30.6 mmol), and the mixture heated to 80 °C for 4 h. The resulting solution was allowed to cool to rt, and the solid formed was removed by filtration, washed with Et<sub>2</sub>O, and dried in vacuo to give the title compound as a white powder (4.97 g, 25.9 mmol, 84%). <sup>1</sup>H NMR (500 MHz, DMSO-*d*<sub>6</sub>): δ 10.30 (s, 1H), 7.26–7.22 (m, 2H), 7.08 (dd, *J* = 1.4 Hz, 7.7 Hz, 1H), 6.69 (dd, *J* = 2.2 Hz, 7.9 Hz, 1H), 3.90 (s, 2H), 3.74 (s, 3H).

***T. cruzi* In Vitro Intracellular Assay.** Compounds were dispensed into black 384-well assay plates (Corning) by acoustic dispensing (LabCyte ECHO). For potency determinations, 10-point one in three dilution curves were generated, with a top concentration of 50 μM. VERO cells were infected overnight with *T. cruzi* trypomastigotes (X10/7) in T225 tissue culture flasks at a multiplicity of infection of 5. Next, any remaining free trypomastigotes were washed away with serum-free MEM media and the infected VERO cells were harvested by trypsinization. The infected VERO cells were then plated into 384-well plates containing the compounds to be tested at 4000 cells per well in MEM media with 1% FCS. After 72 h incubation at 37 °C in the presence of 5% CO<sub>2</sub>, the plates were fixed with 4% formaldehyde for 20 min at room temperature and stained with 5 μg/mL Hoechst 33342. The plates were imaged on a PerkinElmer Operetta high-content imaging system using a 20× objective. Images were analyzed using the Columbus system (PerkinElmer). The image analysis algorithm first identified the VERO nuclei, followed by demarcation of the cytoplasm and identification of intracellular amastigotes. This algorithm reported mean number of parasites per VERO cell and total number of VERO cells.

**TcCYP-51 Assay.** An 11-point dose–response curve of test compound was created using an Echo acoustic dispenser and 200 nL added to a low volume 384-well assay plate. Two dose–response curves for posaconazole were added to this plate as a positive control. To the assay plate, 10 μL of an incubation mixture (containing recombinantly expressed *T. cruzi* CYP51 (final assay conc 37 pmol/mL) and Vivid BOMCC (purchased from Invitrogen, final assay conc 100 μM) was added. Then 10 μL of regenerating cofactor mixture (final conc 2.7 mM glucose-6-phosphate, 0.2 mM NADP, 0.6 units glucose-6-phosphate dehydrogenase and 2% NaHCO<sub>3</sub>) is added, and the reaction is stored at ambient temperature for 1 h. After this time, 2 μL of a stop solution (10 uM posaconazole) was added to terminate any subsequent activity, and the plate was read on a fluorescence plate reader (exc 405 nm, em 450 nm). The % decrease in production of fluorescent product CHC from BOMCC is measured in the presence of each concentration of test compound to provide an IC<sub>50</sub> plot.

**Kinetic Aqueous Solubility Assessment.** The aqueous solubility of test compounds was measured using laser nephelometry. Compounds were subject to serial dilution from 10 to 0.5 mM in DMSO. An aliquot was then mixed with Milli-Q water to obtain an aqueous dilution plate with a final concentration range of 250–12  $\mu\text{M}$ , with a final DMSO concentration of 2.5%. Triplicate aliquots were transferred to a flat-bottomed polystyrene plate, which was immediately read on the NEPHELOstar (BMG Lab Technologies). The amount of laser scatter caused by insoluble particulates (relative nephelometry units, RNU) was plotted against compound concentration using a segmental regression fit, with the point of inflection being quoted as the compounds aqueous solubility ( $\mu\text{M}$ ).

**Solubility of Solid Compounds in Fasted Simulated Intestinal Fluid.** This experiment determines the solubility of solid compounds in fasted simulated intestinal fluid (FaSSIF) at pH 6.5 after 4 h equilibration at room temperature. Then 1 mL of FaSSIF buffer (3 mM sodium taurocholate, 0.75 mM lecithin in sodium phosphate buffer at pH 6.5) was added to manually weighed 1 mg of solid compound in a 2 mL HPLC autosampler vial. The resulting suspension is shaken at 900 rpm for 4 h at room temperature and then transferred to a Multiscreen HTS, 96-well solubility filter plate. The residual solid was removed by filtration. The supernatant solution was quantified by HPLC-UV using single-point calibration of a known concentration of the compound in DMSO. The dynamic range of the assay was 1–1000  $\mu\text{g/mL}$ .

**Measurement of ChiLogD.** A fast gradient, reverse-phase HPLC method was used to determine the chromatographic hydrophobicity index (ChiLogD<sub>7.4</sub>) as devised by Camurri and Zaramella<sup>40</sup> and Valko et al.<sup>41</sup> By plotting the retention time of a set of reference compounds against known Chi values, the Chi value of test compounds can be calculated according to their retention time. Test compounds were prepared as 0.5 mM solutions in 50:50 acetonitrile:water and analyzed by reversed-phase HPLC-UV (wavelength 254 nm) using a Phenomenex Luna C18 100 Å 150 mm  $\times$  4.6 mm 5  $\mu\text{m}$  column with a gradient of aqueous phase (50 mM ammonium acetate (pH 7.4)) and mobile phase (acetonitrile).

**Intrinsic Clearance (Cl<sub>i</sub>) Experiments.** Test compound (0.5  $\mu\text{M}$ ) was incubated with female CD1 mouse liver microsomes (Xenotech LLC; 0.5 mg/mL 50 mM potassium phosphate buffer, pH 7.4) and the reaction started with addition of excess NADPH (8 mg/mL 50 mM potassium phosphate buffer, pH 7.4). Immediately, at time zero, then at 3, 6, 9, 15, and 30 min, an aliquot (50  $\mu\text{L}$ ) of the incubation mixture was removed and mixed with acetonitrile (100  $\mu\text{L}$ ) to stop the reaction. Internal standard was added to all samples, the samples centrifuged to sediment precipitated protein, and the plates then sealed prior to UPLCMSMS analysis using a Quattro Premier XE (Waters Corporation, USA). XLfit (IDBS, UK) was used to calculate the exponential decay, and consequently the rate constant ( $k$ ) from the ratio of peak area of test compound to internal standard at each time point. The rate of intrinsic clearance (Cl<sub>i</sub>) of each test compound was then calculated using the equation  $\text{Cl}_i (\text{mL}/\text{min}/\text{g liver}) = k \times V \times \text{microsomal protein yield}$ , where  $V$  (mL/mg protein) is the incubation volume/mg protein added and microsomal protein yield is taken as 52.5 mg protein/g liver. Verapamil (0.5  $\mu\text{M}$ ) was used as a positive control to confirm acceptable assay performance.

**Plasma Protein Binding Experiments.** In brief, a 96-well equilibrium dialysis apparatus was used to determine the free fraction in mouse plasma for each compound (HT Dialysis LLC, Gales Ferry, CT). Membranes (12–14 kDa cutoff) were conditioned in deionized water for 60 min, followed by conditioning in 80:20 deionized water:ethanol for 20 min and then rinsed in isotonic buffer before use. Female CD1 mouse plasma was removed from the freezer and allowed to thaw on the day of experiment. Thawed plasma was then centrifuged (Allegra X12-R, Beckman Coulter, USA), spiked with test compound (final concentration 10  $\mu\text{g/mL}$ ), and 150  $\mu\text{L}$  aliquots ( $n = 6$  replicate determinations) loaded into the 96-well equilibrium dialysis plate. Dialysis vs isotonic buffer (150  $\mu\text{L}$ ) was carried out for 5 h in a temperature controlled incubator at ca. 37 °C (Barworld scientific Ltd., UK) using an orbital microplate shaker at 100 rpm (Barworld scientific Ltd., UK). At the end of the incubation period, 50  $\mu\text{L}$  aliquots of

plasma or buffer were transferred to micronic tubes (Micronic BV, The Netherlands) and the composition in each tube balanced with control fluid (50  $\mu\text{L}$ ), such that the volume of buffer to plasma was the same. Sample extraction was performed by the addition of 200  $\mu\text{L}$  of acetonitrile containing an appropriate internal standard. Samples were allowed to mix for 1 min and then centrifuged at 3000 rpm in 96-well blocks for 15 min (Allegra X12-R, Beckman Coulter, USA), after which 150  $\mu\text{L}$  of supernatant was removed to 50  $\mu\text{L}$  of water. All samples were analyzed by UPLC-MS/MS on a Quattro Premier XE mass spectrometer (Waters Corporation, USA). The unbound fraction was determined as the ratio of the peak area in buffer to that in plasma.

All Animal Studies Were Ethically Reviewed and Carried out in Accordance with Animals (Scientific Procedures) Act 1986 and the GSK/Dundee University/LSHTM Policy on the Care, Welfare, and Treatment of Animals

**Mouse Pharmacokinetics.** Test compound (11) was dosed as a bolus solution intraperitoneally at 10 mg free base/kg (dose volume, 10 mL/kg; dose vehicle, 5% DMSO/40% PEG400/55% saline) to female NMRI mice ( $n = 3$ ) or dosed orally by gavage as a solution at 10 mg free base/kg (11 [suspension], 13, 20, 37, 48, 58, and 59) to female NMRI mice ( $n = 3$ /dose level) or as suspension at 50 mg of free base/kg (58 and 59) to female balb/c mice (dose volume, 10 mL/kg; dose vehicle, 5% DMSO/40% PEG400/55% distilled water, 20, 48, and 58; or 0.5% w/v hydroxypropylmethylcellulose with 0.4% v/v Tween 80 and 0.5% v/v benzyl alcohol, 11 (10 mg free base/kg), 58 and 59 (50 mg free base/kg). Blood samples were taken from each mouse at 5, 15, and 30 min, 1, 2, 4, 6, 8, and 24 (58 and 59 only) hours postdose and mixed with two volumes of distilled water. After suitable sample preparation, the concentration of test compound in blood was determined by UPLC/MS/MS using a Quattro Premier XE (Waters, USA). Pharmacokinetic parameters were derived from the mean blood concentration time curve using PK solutions software v 2.0 (Summit Research Services, USA).

**In Vivo Testing and Bioluminescence Imaging.** Female BALB/c (Charles River; UK), aged 8–12 weeks, were infected with bioluminescent *T. cruzi* (CL Brener) expressing the firefly luciferase *PpyRE9h* gene.<sup>65</sup> Typically, 10<sup>4</sup> bloodstream trypomastigotes (BTs) in 0.2 mL of PBS were first used to infect SCID mice via intraperitoneal (ip) inoculation. Parasitaemic blood from these mice was obtained 2–3 weeks later and adjusted to  $5 \times 10^3$  BTs mL<sup>-1</sup> with PBS. The infection of BALB/c mice was by ip inoculation with  $1 \times 10^3$  BTs. Treatment was initiated 14 (acute stage) or 97 (chronic stage) days postinfection. Drugs were administered by oral gavage (~200  $\mu\text{L}$ ), and vehicle only (0.5% w/v hydroxypropylmethylcellulose with 0.4% v/v Tween 80 and 0.5% v/v benzyl alcohol) was administered to control mice. Following the first daily dose on day 1 and day 21, a blood sample was taken from all drug treated mice predose, then 30 min, 1, 2, 4, and 8 h postdose, mixed with two volumes of distilled water and analyzed for test compound as for mouse pharmacokinetics above. To detect residual infection, mice were immunosuppressed with cyclophosphamide (200 mg/kg) by ip injection every 4 days for a maximum of three doses.

For in vivo imaging, mice were injected ip with 150 mg/kg D-luciferin in Dulbecco's Ca<sup>2+</sup>/Mg<sup>2+</sup> free PBS, then anaesthetized using 2.5% (v/v) isoflurane in oxygen. Images were obtained using an IVIS Lumina II system (Caliper Life Science) 10–20 min after D-luciferin administration. The detection threshold was established from uninfected mice. Organs/tissue samples were assessed by ex vivo imaging as described previously.<sup>65</sup>

## ■ ASSOCIATED CONTENT

### Supporting Information

The Supporting Information is available free of charge on the ACS Publications website at DOI: 10.1021/acs.jmedchem.7b00463.

This contains synthetic details for all compounds in the main body of the paper, supplementary data tables, more information on ADMET and pharmacology (PDF)

Molecular formula strings (CSV)

## AUTHOR INFORMATION

### Corresponding Authors

\*For I.H.G.: phone, +44 1382 386 240; E-mail, [i.h.gilbert@dundee.ac.uk](mailto:i.h.gilbert@dundee.ac.uk).

\*For T.J.M.: phone, +34 650 349 771; E-mail, [tim.j.miles@gsk.com](mailto:tim.j.miles@gsk.com).

\*For K.D.R.: phone, +44 1382 388 688; E-mail, [k.read@dundee.ac.uk](mailto:k.read@dundee.ac.uk).

### ORCID

Manu De Rycker: 0000-0002-3171-3519

Ian H. Gilbert: 0000-0002-5238-1314

### Notes

The authors declare no competing financial interest.

## ACKNOWLEDGMENTS

Funding for this work was provided by the Wellcome Trust (nos. 092340 and 100476). We thank Gina MacKay for performing HRMS analyses and for assistance with performing other NMR and MS analyses, Alastair Pate and Francesco Gastaldello for data management, Lorna Campbell and Irene Hallyburton for performing HepG2 assays and plasmodium parasite assays, and Dr. Stephen Patterson for critical evaluation of the manuscript.

## ABBREVIATIONS USED

ATC, 5-amino-1,2,3-triazole-4-carboxamide; BNZ, benznidazole; PFI, property forecast index; eXP, GSK enhanced cross-screen panel

## REFERENCES

- (1) Rassi, A., Jr.; Rassi, A.; Marin-Neto, J. A. Chagas disease. *Lancet* **2010**, *375*, 1388–1402.
- (2) Bocchi, E. A. Heart failure in South America. *Curr. Cardiol. Rev.* **2013**, *9*, 147–156.
- (3) Martins-Melo, F. R.; Alencar, C. H.; Ramos, A. N., Jr.; Heukelbach, J. Epidemiology of mortality related to Chagas' disease in Brazil, 1999–2007. *PLoS Neglected Trop. Dis.* **2012**, *6*, e1508.
- (4) Bonney, K. M. Chagas disease in the 21st century: a public health success or an emerging threat? *Parasite* **2014**, *21*, 11.
- (5) Giddings, O. K.; Eickhoff, C. S.; Smith, T. J.; Bryant, L. A.; Hoft, D. F. Anatomical route of invasion and protective mucosal immunity in *Trypanosoma cruzi* conjunctival infection. *Infect. Immun.* **2006**, *74*, 5549–5560.
- (6) Nickerson, P.; Orr, P.; Schroeder, M. L.; Sekla, L.; Johnston, J. B. Transfusion-associated *Trypanosoma cruzi* infection in a non-endemic area. *Ann. Intern. Med.* **1989**, *111*, 851–853.
- (7) Nobrega, A. A.; Garcia, M. H.; Tatto, E.; Obara, M. T.; Costa, E.; Sobel, J.; Araujo, W. N. Oral transmission of Chagas' disease by consumption of acai palm fruit, Brazil. *Emerging Infect. Dis.* **2009**, *15*, 653–655.
- (8) Nowicki, M. J.; Chinchilla, C.; Corado, L.; Matsuoka, L.; Selby, R.; Steurer, F.; Mone, T.; Mendez, R.; Aswad, S. Prevalence of antibodies to *Trypanosoma cruzi* among solid organ donors in southern California: a population at risk. *Transplantation* **2006**, *81*, 477–479.
- (9) Norman, F. F.; Lopez-Velez, R. Chagas disease and breast-feeding. *Emerging Infect. Dis.* **2013**, *19*, 1561–1566.
- (10) Coura, J. R.; Vinas, P. A. Chagas disease: a new worldwide challenge. *Nature* **2010**, *465*, S6–7.
- (11) Dias, J. C. The indeterminate form of human chronic Chagas' disease: a clinical epidemiological review. *Rev. Soc. Bras. Med. Trop.* **1989**, *22*, 147–156.
- (12) Bustamante, J. M.; Rivarola, H. W.; Fernandez, A. R.; Enders, J. E.; Fretes, R.; Palma, J. A.; Paglini-Oliva, P. A. Indeterminate Chagas' disease: *Trypanosoma cruzi* strain and re-infection are factors involved in the progression of cardiopathy. *Clin. Sci.* **2003**, *104*, 415–420.

(13) Koberle, F. Chagas' disease and Chagas' syndromes: the pathology of American trypanosomiasis. *Adv. Parasitol.* **1968**, *6*, 63–116.

(14) Prata, A. Clinical and epidemiological aspects of Chagas' disease. *Lancet Infect. Dis.* **2001**, *1*, 92–100.

(15) Bern, C.; Montgomery, S. P.; Herwaldt, B. L.; Rassi, A., Jr.; Marin-Neto, J. A.; Dantas, R. O.; Maguire, J. H.; Acquatella, H.; Morillo, C.; Kirchhoff, L. V.; Gilman, R. H.; Reyes, P. A.; Salvatella, R.; Moore, A. C. Evaluation and treatment of Chagas disease in the United States: a systematic review. *JAMA, J. Am. Med. Assoc.* **2007**, *298*, 2171–2181.

(16) Castro, J. A.; de Mecca, M. M.; Bartel, L. C. Toxic side effects of drugs used to treat Chagas' disease (American trypanosomiasis). *Hum. Exp. Toxicol.* **2006**, *25*, 471–479.

(17) Le Loup, G.; Pialoux, G.; Lescure, F. X. Update in treatment of Chagas' disease. *Curr. Opin. Infect. Dis.* **2011**, *24*, 428–434.

(18) Molina, I.; Gomez i Prat, J.; Salvador, F.; Trevino, B.; Sulleiro, E.; Serre, N.; Pou, D.; Roure, S.; Cabezos, J.; Valerio, L.; Blanco-Grau, A.; Sanchez-Montalva, A.; Vidal, X.; Pahissa, A. Randomized trial of posaconazole and benznidazole for chronic Chagas' disease. *N. Engl. J. Med.* **2014**, *370*, 1899–1908.

(19) Torrico, F., E1224—results of proof of concept clinical trial in patients with chronic indeterminate Chagas disease. *Proceedings of the 62nd Annual Meeting of the American Society of Tropical Medicine and Hygiene, Washington, DC, November 13–17, 2013*, 2013.

(20) Morillo, C. A.; Marin-Neto, J. A.; Avezum, A.; Sosa-Estani, S.; Rassi, A.; Rosas, F.; Villena, E.; Quiroz, R.; Bonilla, R.; Britto, C.; Guhl, F.; Velazquez, E.; Bonilla, L.; Meeks, B.; Rao-Melacini, P.; Pogue, J.; Mattos, A.; Lazdins, J.; Rassi, A.; Connolly, S. J.; Yusuf, S. Investigators, B. Randomized trial of benznidazole for chronic Chagas' cardiomyopathy. *N. Engl. J. Med.* **2015**, *373*, 1295–1306.

(21) Brenk, R.; Schipani, A.; James, D.; Krasowski, A.; Gilbert, I. H.; Frearson, J.; Wyatt, P. G. Lessons learnt from assembling screening libraries for drug discovery for neglected diseases. *ChemMedChem* **2008**, *3*, 435–444.

(22) De Rycker, M.; Thomas, J.; Riley, J.; Brough, S. J.; Miles, T. J.; Gray, D. W. Identification of trypanocidal activity for known clinical compounds using a new *Trypanosoma cruzi* hit-discovery screening cascade. *PLoS Neglected Trop. Dis.* **2016**, *10*, e0004584.

(23) Hopkins, A. L.; Groom, C. R.; Alex, A. Ligand efficiency: a useful metric for lead selection. *Drug Discovery Today* **2004**, *9*, 430–431.

(24) Hopkins, A. L.; Keseru, G. M.; Leeson, P. D.; Rees, D. C.; Reynolds, C. H. The role of ligand efficiency metrics in drug discovery. *Nat. Rev. Drug Discovery* **2014**, *13*, 105–121.

(25) Kaiser, M.; Maser, P.; Tadoori, L. P.; Ioset, J. R.; Brun, R. Antiprotozoal activity profiling of approved drugs: a starting point toward drug repositioning. *PLoS One* **2015**, *10*, e0135556.

(26) Avelar, L. A. A.; Camilo, C. D.; de Albuquerque, S.; Fernandes, W. B.; Goncalves, C.; Kenny, P. W.; Leitao, A.; McKerrow, J. H.; Montanari, C. A.; Orozco, E. V. M.; Ribeiro, J. F. R.; Rocha, J. R.; Rosini, F.; Saidel, M. E. Molecular design, synthesis and trypanocidal activity of dipeptidyl nitriles as cruzain inhibitors. *PLoS Neglected Trop. Dis.* **2015**, *9*, e0003916.

(27) Menezes, J. C. L.; Vaz, L. B. A.; de Abreu Vieira, P. M.; da Silva Fonseca, K. D.; Carneiro, C. M.; Taylor, J. G. Synthesis and anti-*Trypanosoma cruzi* activity of diaryldiazepines. *Molecules* **2015**, *20*, 43–51.

(28) Germain, A. R.; Carmody, L. C.; Dockendorff, C.; Galan-Rodriguez, C.; Rodriguez, A.; Johnston, S.; Bittker, J. A.; MacPherson, L.; Dandapani, S.; Palmer, M.; Schreiber, S. L.; Munoz, B. Identification of small-molecule inhibitors of *Trypanosoma cruzi* replication. *Bioorg. Med. Chem. Lett.* **2011**, *21*, 7197–7200.

(29) Keenan, M.; Chaplin, J. H.; Alexander, P. W.; Abbott, M. J.; Best, W. M.; Khong, A.; Botero, A.; Perez, C.; Cornwall, S.; Thompson, R. A.; White, K. L.; Shackelford, D. M.; Koltun, M.; Chiu, F. C. K.; Morizzi, J.; Ryan, E.; Campbell, M.; von Geldern, T. W.; Scandale, I.; Chatelain, E.; Charman, S. A. Two analogues of

fenarimol show curative activity in an experimental model of Chagas' disease. *J. Med. Chem.* **2013**, *56*, 10158–10170.

(30) Neitz, R. J.; Chen, S.; Supek, F.; Yeh, V.; Kellar, D.; Gut, J.; Bryant, C.; Gallardo-Godoy, A.; Molteni, V.; Roach, S. L.; Chatterjee, A. K.; Robertson, S.; Renslo, A. R.; Arkin, M.; Glynn, R.; McKerrow, J.; Siqueira-Neto, J. L. Lead identification to clinical candidate selection: drugs for Chagas' disease. *J. Biomol. Screening* **2015**, *20*, 101–111.

(31) Nwaka, S.; Besson, D.; Ramirez, B.; Maes, L.; Matheeußen, A.; Bickle, Q.; Mansour, N. R.; Yousif, F.; Townson, S.; Gokool, S.; Chongwa, F.; Samje, M.; Misra-Bhattacharya, S.; Murthy, P. K.; Fakorede, F.; Paris, J. M.; Yeates, C.; Ridley, R.; Van Voorhis, W. C.; Geary, T. Integrated dataset of screening hits against multiple neglected disease pathogens. *PLoS Neglected Trop. Dis.* **2011**, *5*, e1412.

(32) Katsuno, K.; Burrows, J. N.; Duncan, K.; van Huijsduijnen, R. H.; Kaneko, T.; Kita, K.; Mowbray, C. E.; Schmatz, D.; Warner, P.; Slingsby, B. T. Hit and lead criteria in drug discovery for infectious diseases of the developing world. *Nat. Rev. Drug Discovery* **2015**, *14*, 751–758.

(33) Chatelain, E. Chagas disease drug discovery: toward a new era. *J. Biomol. Screening* **2015**, *20*, 22–35.

(34) Edwards, M. P.; Price, D. A. Role of physicochemical properties and ligand lipophilicity efficiency in addressing drug safety risks. *Annu. Rep. Med. Chem.* **2010**, *45*, 380–391.

(35) Freeman-Cook, K. D.; Hoffman, R. L.; Johnson, T. W. Lipophilic efficiency: the most important efficiency metric in medicinal chemistry. *Future Med. Chem.* **2013**, *5*, 113–115.

(36) Kiselyov, A. S.; Semenova, M.; Semenov, V. V. (1,2,3-Triazol-4-yl)benzenamines: synthesis and activity against VEGF receptors 1 and 2. *Bioorg. Med. Chem. Lett.* **2009**, *19*, 1344–1348.

(37) Levin, J. I.; Turos, E.; Weinreb, S. M. An alternative procedure for the aluminium-mediated conversion of esters to amides. *Synth. Commun.* **1982**, *12*, 989–993.

(38) Goddard-Borger, E. D.; Stick, R. V. An efficient, inexpensive, and shelf-stable diazotransfer reagent: imidazole-1-sulfonyl azide hydrochloride. *Org. Lett.* **2007**, *9*, 3797–3800.

(39) Mannhold, R.; Dross, K. Calculation procedures for molecular lipophilicity: a comparative study. *Quant. Struct.-Act. Relat.* **1996**, *15*, 403–409.

(40) Camurri, G.; Zaramella, A. High-throughput liquid chromatography/mass spectrometry method for the determination of the chromatographic hydrophobicity index. *Anal. Chem.* **2001**, *73*, 3716–3722.

(41) Valko, K.; Nunhuck, S.; Bevan, C.; Abraham, M. H.; Reynolds, D. P. Fast gradient HPLC method to determine compounds binding to human serum albumin. Relationships with octanol/water and immobilized artificial membrane lipophilicity. *J. Pharm. Sci.* **2003**, *92*, 2236–2248.

(42) Leeson, P. D.; Young, R. J. Molecular property design: does everyone get it? *ACS Med. Chem. Lett.* **2015**, *6*, 722–725.

(43) Young, R. J.; Green, D. V. S.; Luscombe, C. N.; Hill, A. P. Getting physical in drug discovery II: the impact of chromatographic hydrophobicity measurements and aromaticity. *Drug Discovery Today* **2011**, *16*, 822–830.

(44) Bastin, R. J.; Bowker, M. J.; Slater, B. J. Salt selection and optimization procedures for pharmaceutical new chemical entities. *Org. Process Res. Dev.* **2000**, *4*, 427–435.

(45) Bows, J.; Brown, A. J.; Hamon, J.; Jarolimek, W.; Sridhar, A.; Waldron, G.; Whitebread, S. Reducing safety-related drug attrition: the use of in vitro pharmacological profiling. *Nat. Rev. Drug Discovery* **2012**, *11*, 909–922.

(46) Kargl, J.; Brown, A. J.; Andersen, L.; Dorn, G.; Schicho, R.; Waldhoer, M.; Heinemann, A. A selective antagonist reveals a potential role of G protein-coupled receptor 55 in platelet and endothelial cell function. *J. Pharmacol. Exp. Ther.* **2013**, *346*, 54–66.

(47) Priest, B. T.; Bell, I. M.; Garcia, M. L. Role of hERG potassium channel assays in drug development. *Channels* **2008**, *2*, 87–93.

(48) Jones, K. A.; Garbati, N.; Zhang, H.; Large, C. H. In *High Throughput Screening: Methods and Protocols*, 2nd ed.; Janzen, W. P.,

Bernasconi, P., Eds.; Humana Press: Totowa, NJ, 2009; Vol. 565, 209–223.

(49) Haworth, S.; Lawlor, T.; Mortelmans, K.; Speck, W.; Zeiger, E. Salmonella mutagenicity test-results for 250 chemicals. *Environ. Mutagen.* **1983**, *5*, 3–49.

(50) Brown, N. Bioisosteres and scaffold hopping in medicinal chemistry. *Mol. Inf.* **2014**, *33*, 458–462.

(51) Junge, W.; Krisch, K.; Conney, A. The carboxylesterases/amidases of mammalian liver and their possible significance. *Crit. Rev. Toxicol.* **1975**, *3*, 371–434.

(52) Borosky, G. L. Quantum-chemical studies on mutagenicity of aromatic and heteroaromatic amines. *Front. Biosci., Scholar Ed.* **2013**, *S5*, 600–610.

(53) Jamieson, C.; Moir, E. M.; Rankovic, Z.; Wishart, G. Medicinal chemistry of hERG optimizations: highlights and hang-ups. *J. Med. Chem.* **2006**, *49*, 5029–5046.

(54) Shamovsky, I.; Ripa, L.; Borjesson, L.; Mee, C.; Norden, B.; Hansen, P.; Hasselgren, C.; O'Donovan, M.; Sjo, P. Explanation for main features of structure-genotoxicity relationships of aromatic amines by theoretical studies of their activation pathways in CYP1A2. *J. Am. Chem. Soc.* **2011**, *133*, 16168–16185.

(55) Lepesheva, G. I.; Villalta, F.; Waterman, M. R. Targeting *Trypanosoma cruzi* sterol 14 $\alpha$ -demethylase (CYP51). *Adv. Parasitol.* **2011**, *75*, 65–87.

(56) Gunatilleke, S. S.; Calvet, C. M.; Johnston, J. B.; Chen, C. K.; Erenburg, G.; Gut, J.; Engel, J. C.; Ang, K. K.; Mulvaney, J.; Chen, S.; Arkin, M. R.; McKerrow, J. H.; Podust, L. M. Diverse inhibitor chemotypes targeting *Trypanosoma cruzi* CYP51. *PLoS Neglected Trop. Dis.* **2012**, *6*, e1736.

(57) Keenan, M.; Alexander, P. W.; Chaplin, J. H.; Abbott, M. J.; Diao, H.; Wang, Z.; Best, W. M.; Perez, C. J.; Cornwall, S. M.; Keatley, S. K.; Thompson, R. C.; Charman, S. A.; White, K. L.; Ryan, E.; Chen, G.; Ioset, J. R.; von Geldern, T. W.; Chatelain, E. Selection and optimization of hits from a high-throughput phenotypic screen against *Trypanosoma cruzi*. *Future Med. Chem.* **2013**, *5*, 1733–1752.

(58) Friggeri, L.; Scipione, L.; Costi, R.; Kaiser, M.; Moraca, F.; Zamperini, C.; Botta, B.; Di Santo, R.; De Vita, D.; Brun, R.; Tortorella, S. New promising compounds with in vitro nanomolar activity against *Trypanosoma cruzi*. *ACS Med. Chem. Lett.* **2013**, *4*, 538–541.

(59) Andriani, G.; Amata, E.; Beatty, J.; Clements, Z.; Coffey, B. J.; Courtemanche, G.; Devine, W.; Erath, J.; Juda, C. E.; Wawrzak, Z.; Wood, J. T.; Lepesheva, G. I.; Rodriguez, A.; Pollastri, M. P. Antitrypanosomal lead discovery: identification of a ligand-efficient inhibitor of *Trypanosoma cruzi* CYP51 and parasite growth. *J. Med. Chem.* **2013**, *56*, 2556–2567.

(60) Alonso-Padilla, J.; Rodriguez, A. High throughput screening for anti-*Trypanosoma cruzi* drug discovery. *PLoS Neglected Trop. Dis.* **2014**, *8*, e3259.

(61) Pena, I.; Pilar Manzano, M.; Cantizani, J.; Kessler, A.; Alonso-Padilla, J.; Bardera, A. I.; Alvarez, E.; Colmenarejo, G.; Cutillo, I.; Roquero, I.; de Dios-Anton, F.; Barroso, V.; Rodriguez, A.; Gray, D. W.; Navarro, M.; Kumar, V.; Sherstnev, A.; Drewry, D. H.; Brown, J. R.; Fiandor, J. M.; Julio Martin, J. New compound sets identified from high throughput phenotypic screening against three kinetoplastid parasites: an open resource. *Sci. Rep.* **2015**, *5*, 8771.

(62) Riley, J.; Brand, S.; Voice, M.; Caballero, I.; Calvo, D.; Read, K. D. Development of a fluorescence-based *Trypanosoma cruzi* CYP51 inhibition assay for effective compound triaging in drug discovery programmes for Chagas' disease. *PLoS Neglected Trop. Dis.* **2015**, *9*, e0004014.

(63) Kalgutkar, A. S.; Obach, R. S.; Maurer, T. S. Mechanism-based inactivation of cytochrome P450 enzymes: chemical mechanisms, structure-activity relationships and relationship to clinical drug-drug interactions and idiosyncratic adverse drug reactions. *Curr. Drug Metab.* **2007**, *8*, 407–447.

(64) Zingales, B.; Miles, M. A.; Moraes, C. B.; Luquetti, A.; Guhl, F.; Schijman, A. G.; Ribeiro, I. Drug discovery for Chagas' disease should



consider *Trypanosoma cruzi* strain diversity. *Mem. Inst. Oswaldo Cruz* **2014**, *109*, 828–833.

(65) Francisco, A. F.; Lewis, M. D.; Jayawardhana, S.; Taylor, M. C.; Chatelain, E.; Kelly, J. M. Limited ability of posaconazole to cure both acute and chronic *Trypanosoma cruzi* infections revealed by highly sensitive in vivo imaging. *Antimicrob. Agents Chemother.* **2015**, *59*, 4653–4661.